Hydrological Processes

WILEY

RESEARCH ARTICLE

Karst Hydrologic Memory Supplements Streamflow During Dry Periods in Snow-Dominated, Mountainous Watersheds

Hyrum Tennant[1] | Bethany T. Neilson[1] | Devon Hill[1] | Dennis L. Newell[2] | James P. Evans[2] | Seohye Choi[3] | James P. McNamara[4] | Nathaniel Ashmead[4] | Tianfang Xu[3]

[1]Civil and Environmental Engineering, Utah Water Research Laboratory, Utah State University, Logan, Utah, USA | [2]Department of Geosciences, Utah State University, Logan, Utah, USA | [3]School of Sustainable Engineering and the Built Environment, Arizona State University, Tempe, Arizona, USA | [4]Department of Geoscience, Boise State University, Boise, Idaho, USA

Correspondence: Hyrum Tennant (hyrum.tennant@usu.edu)

Received: 31 May 2024 | **Revised:** 19 November 2024 | **Accepted:** 20 November 2024

Funding: This work was supported by the National Science Foundation, Utah Water Research Laboratory, Utah State University.

Keywords: drought | groundwater storage | Intermountain West | karst aquifer | karst memory | low-flows | snow-dominated watersheds | streamflow regimes | water management

ABSTRACT

Analysis of PRISM and SNOTEL station data paired with USGS streamflow gage data in the western United States shows that, in snow-dominated mountainous watersheds, streamflow regimes differ between watersheds with karst geology and their non-karst neighbours. These carbonate aquifers exhibit a spectrum of flow paths encompassing karst conduits, including large fractures or voids that transmit water readily to springs and other surface waters, and matrix flow paths through soils, highly fractured bedrock, or porous media bedrock grains. A well-connected karst aquifer will discharge a large portion of its accumulated precipitation to surface water via springs and other groundwater flow paths on an annual scale, exhibiting a lagged response to precipitation presenting as a "memory effect" in hydrograph time series. These patterns were observed in the hydrologic records of gaged watersheds with exposed or near-surface carbonate layers accounting for > 30% of their drainage area. In western snow-dominated watersheds, where paired streamflow and SNOTEL data are available, analysis of the precipitation and flow time series shows low-flow volume is strongly related to karst aquifer conditions and winter precipitation when compared to low-flow volumes present in non-karst watersheds, which have a complex relationship to multiple driving metrics. Analysis of normalised streamflow and cumulative precipitation in karst watersheds show that low-flow conditions are highly dependent on the preceding winter precipitation and streamflow in both wet and dry periods. In non-karst watersheds, increased precipitation primarily impacts high-flow, spring runoff volumes with no clear relationship to low-flow periods. When comparing cumulative streamflow and precipitation volumes within each water year and over longer timescales, karst watersheds show the potential filling and draining of large amounts of karst storage, whereas non-karst watersheds demonstrate a more stable storage regime. Communities in many western US watersheds are dependent on snow-dominated karst watersheds for their water supply. This analysis, using widely available hydrologic data, can provide insight into the recharge and storage processes within these watersheds, improve our ability to assess current flow regimes, anticipate the impacts of climate change on water availability, and help manage water supplies.

1 | Introduction

The Intermountain West region in the U.S. is characterised by a semi-arid climate with hydrological regimes driven by winter snowfall and dry summers. These areas are highly dependent on surface water sources (rivers, and reservoirs) for their water supply. The US Geological Survey estimates that approximately 65% of water withdrawals in Intermountain West states are sourced from surface water. In Utah, Nevada, Idaho, and Arizona, 73%, 51%, 70%, and 54% of total withdrawals are sourced from surface water, respectively (Dieter et al. 2018). Many watersheds in this region contain karst aquifers characterised by heterogeneous distributions of sinkholes, conduits, and caves, offering the potential for substantial groundwater storage (Bakalowicz 2005; Ford and Williams 2013; Pulido-Bosch 2021; Sloto, Cecil, and Senior 1991). Some of the primary groundwater flow paths connecting karst aquifers to surface water can have significantly shorter residence times compared to those in non-karst watersheds (Freeze and Cherry 1979; Worthington, Schindel, and Alexander Jr 2002). Longer residence time flow paths, including flow through soils, fractured bedrock, or porous media bedrock grains, will be defined as matrix flow paths herein (Brooks et al. 2015; Godsey, Kirchner, and Tague 2014; Liu, Williams, and Caine 2004; Liu et al. 2008; Somers and McKenzie 2020; Winter 1995). The additional groundwater contributions to rivers and streams via karst flow paths can significantly influence surface water hydrologic regimes where karst geology underlies a significant proportion of the watershed (Kresic 2012; Winter 1995). In karst watersheds where surface water is a critical component of the local water supply, understanding the effects of karst flow paths on the streamflow regimes can lead to more effective water resource management.

Streamflow regimes in western US watersheds are framed by the rapid melt of winter snowpack producing spring runoff (Bales et al. 2006; Barnhart et al. 2016; Dettinger, Udall, and Georgakakos 2015; Knowles, Dettinger, and Cayan 2006; Rumsey, Miller, and Sexstone 2020). Spring runoff results in multiple orders of magnitude increase in streamflow followed by a recession back to baseflow (Dettinger, Udall, and Georgakakos 2015; Hammond, Saavedra, and Kampf 2018; Knowles, Dettinger, and Cayan 2006; Rumsey, Miller, and Sexstone 2020). Baseflow in snowmelt-dominated mountain watersheds is typically defined as being sourced from groundwater flow paths due to the lack of precipitation and minimal snowmelt post-spring runoff (Miller et al. 2014; Rimmer and Salingar 2006; Winter 1995). The large storage volume in karst aquifers allows them to capture a significant fraction of snowmelt during spring runoff (Land and Timmons 2016; Meeks and Hunkeler 2015; Spellman et al. 2022) and attenuate runoff patterns non-linearly across a range of timescales (Atkinson 1977; Labat, Mangin, and Ababou 2002). This phenomenon is referred to as the "memory effect" and results from the currently observed baseflow condition being a combined signal from recent precipitation and the prior baseflow condition (Iliopoulou et al. 2019; Mangin 1984; Nippgen et al. 2016).

Climate change is shifting precipitation regimes away from snowmelt-dominated towards more rainfall-dominated in the Intermountain West (Dettinger, Udall, and Georgakakos 2015; Ficklin, Robeson, and Knouft 2016; Knowles, Dettinger, and Cayan 2006). It is unknown how changes in precipitation and snowmelt patterns will affect recharge, karst/matrix contributions, and storage in karst watersheds, particularly given the potential for the continuation of the millennial-scale drought (Segura 2021; Sexstone et al. 2018). Therefore, there is a clear need to understand controlling hydrologic variables and the role of karst geology in modulating the effects of varied precipitation on western watershed streamflow.

In water resources management, planning decisions are often made on a water year scale utilising predictive models. These models typically employ multi-linear regression (MLR) equations using various hydrological variables to generate streamflow forecasts (Garen 1992; Vogel, Wilson, and Daly 1999; Wolf et al. 2023). These hydrological variables represent climate and/or watershed processes in streamflow generation (Fleming and Goodbody 2019; Vogel, Wilson, and Daly 1999). These models do not explicitly measure or incorporate variables representing groundwater storage and its contribution to streamflow, nor do they account for the impact of karst geology (Donovan et al. 2022; Jones et al. 2019; Land and Timmons 2016; Tennant, Crosby, and Godsey 2015). The anticipated continued shift in precipitation phase and patterns in the Intermountain West (Ficklin, Robeson, and Knouft 2016; Rumsey, Miller, and Sexstone 2020; Tennant, Crosby, and Godsey 2015) and the limited work on understanding the impacts of karst geology in these watersheds has led to significant limitations in our ability to predict shifts in streamflow regime.

To anticipate changes in streamflow regimes, we need to identify the significant hydrological variables for understanding karst watersheds and contrast them with our foundational understanding of non-karst watersheds. To address this need, we focus on identifying the key hydrologic factors that control runoff and baseflow generation in snowmelt-dominant karst and non-karst watersheds using MLR methods (Garen 1992; Vogel, Wilson, and Daly 1999). We use variables derived from classical hydrologic metrics over characteristic periods to establish which variables exhibit the best relationship with high-flow volumes during spring runoff and low-flow volumes during baseflow conditions. These hydrologic metrics do not include any direct measures of groundwater conditions. By comparing the variables correlated with high-flow and low-flow volumes in these different watershed classifications, we can identify fundamental differences in the factors that control karst versus non-karst hydrologic regimes. Furthermore, we develop simple predictive regression models specific to each watershed based on hydrologic conditions prior to high and low flow periods to anticipate volumes during critical times.

2 | Methods

We compared hydrologic metrics among seven watersheds in northern Utah and southeastern Idaho to determine if trends in streamflow metrics exist between karst and non-karst watersheds. Additionally, characteristic hydrologic variables were analysed using MLR to determine the hydrologic metrics and periods with the strongest relationships to low-flow and high-flow volumes. Further, simple MLR equations for predicting high-flow and low-flow volumes were established using variables

measured over a period prior to the high-flow or low-flow period to facilitate planning.

2.1 | Study Area

To minimise variability due to differing climate and hydrologic responses and timing, we examined seven snow-dominant watersheds in northern Utah and southeastern Idaho (Figure 1) that all have paired SNOTEL and United States Geological Survey (USGS) stream gaging stations. SNOTEL stations are automated snowpack and climate sensors operated in the western U.S. by the Natural Resources Conservation Service (NRCS), an agency of the United States Department of Agriculture, that provides publicly available data. The USGS operates and provides publicly available data for stream gages across the United States. In this analysis, SNOTEL station and USGS stream gage datasets were required to have at least 20 years of daily data and report data year-round. To avoid human storage influences, all selected watersheds have a reservoir design capacity that is less than 10% of the median total streamflow volume in a water year to ensure limited influence on streamflow regimes. Further, they have karst coverage ranging from 0% to 71% as defined by the presence of surface-exposed carbonate rock calculated from the national karst map (Doctor et al. 2020). Two watersheds, the Logan River and Blacksmith Fork River are in the Idaho-Utah Bear River Range characterised by limestone and dolomite with some siltstone and quartzite intervals. Two watersheds, Red Butte Creek and American Fork are composed primarily of limestone formations and quartz sandstone units, in Utah's Wasatch Range. Three watersheds, Bear River-Stillwater Fork (quartz sandstone with boulder till), Weber River (predominantly quartz sandstone interspersed with limestone formations), and Lake Fork (quartzite and quartz sandstone), are in Utah's Uintah Range (Figure 1). Table S1 includes information on the SNOTEL stations and USGS gaging stations used in each

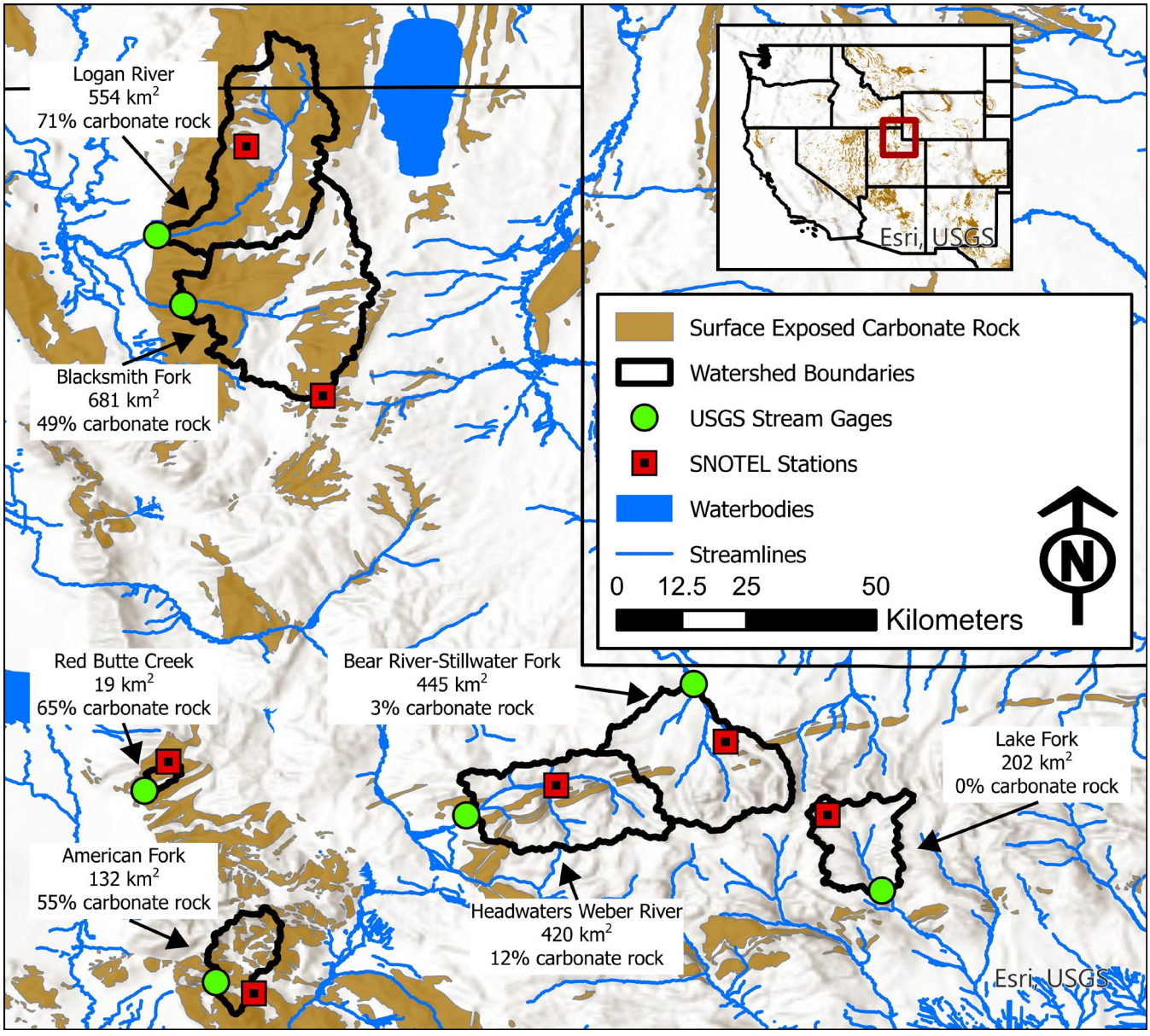

FIGURE 1 | USGS stream gages and SNOTEL stations in selected watersheds for analysis. Surface exposed carbonate rock, shown in orange, is given as a percentage of watershed area.

watershed, while Table S2 provides details on the reservoir storage upstream of each gage (U.S. Army Corps of Engineers 2024).

2.2 | Data

The watershed area for each stream gage was delineated in ArcGIS Pro using USGS 10-m DEMs (Gesch et al. 2018). The surface carbonate rock area for each watershed was determined using a nationwide layer provided by Doctor et al. (2020). Daily SNOTEL data, USGS streamflow data, and site metadata were acquired for each site from the National Water Information System (U.S. Geological Survey 2016). The publicly available 4-km gridded PRISM data (The PRISM Climate Group 2024) was used to derive watershed area-weighted values for precipitation (*Precip.*) and air temperature (*Air Temp.*). Streamflow data include daily averaged flow (m^3s^{-1}). Daily streamflow in cm (q) was determined by dividing the daily flow volume by the watershed area to aid in comparisons between different-sized watersheds. SNOTEL data included daily snow-adjusted precipitation (*PRCPSA*) and daily snow water equivalent (*SWE*) (Table 1). Using *PRCPSA* and *SWE*, daily snowmelt (*Snowmelt*), daily rainfall (*Rain*), and daily snowfall (*Snow*) were calculated for each SNOTEL station.

The Logan River has two gaged diversions upstream of the USGS gage, the Highline Canal (U.S. Geological Survey 2024) and Dewitt Springs (Utah Division of Water Rights 2024). The reported daily average flow from these diversions was added to the streamflow reported at the USGS gage to represent the total streamflow of the Logan River.

2.3 | Characteristic Metrics and Periods

Past work in the Intermountain West has shown that certain hydrologic characteristic metrics measured over hydrologic periods are good predictors of streamflow (Brooks et al. 2021; Wolf et al. 2023). A pool of variables for evaluation using MLR was derived by parsing characteristic hydrologic metrics across significant hydrologic periods (Table 1; Figure 2).

The period between October 1st and the start of spring runoff exhibits relatively consistent streamflow because the streamflow is predominantly composed of baseflow over this period (Ficklin, Robeson, and Knouft 2016; Miller et al. 2014; Rumsey, Miller, and Sexstone 2020). Streamflow recorded during this *low-flow* period is assumed to be representative of the aquifer(s) storage condition (Neilson et al. 2018; Rimmer and Salingar 2006; Rumsey, Miller, and Sexstone 2020; Wolf et al. 2023).

The *high-flow* period, between the start of spring runoff and October 1st, captures a majority of the peak in streamflow due to spring snowmelt in the western U.S. (Barnhart et al. 2016; Hammond, Saavedra, and Kampf 2018; Harrison et al. 2021; Miller et al. 2014; Neilson et al. 2018; Rumsey, Miller, and Sexstone 2020). The correlation between winter precipitation and streamflow during the *high-flow* period is typically quite strong in watersheds in the Intermountain West (Dettinger, Udall, and Georgakakos 2015; Rumsey, Miller, and Sexstone 2020; Stewart,

TABLE 1 | Hydrologic characteristic metrics and hydrologic periods (Figure 2).

Metric	Description	Units
Daily streamflow in cm (q)	Cumulative Daily streamflow volume divided by watershed area.	cm day^{-1}
Daily snow and rain measured as depth of water (*PRCPSA*)	Daily precipitation measured by a precipitation bucket adjusted for snow undercatch at SNOTEL station.	cm day^{-1}
Daily precipitation (*Precip.*)	Average daily precipitation across the watershed from PRISM.	cm day^{-1}
Snow water equivalent (*SWE*)	Depth of water contained in snow measured by a snow pillow at a SNOTEL station.	cm
Daily rainfall (*Rain*)	Daily rainfall measured by a precipitation bucket at a SNOTEL station.	cm day^{-1}
Daily snowfall (*Snow*)	Daily snowfall measured by a snow pillow measured as depth of water at a SNOTEL station.	cm day^{-1}
Daily snowmelt (*Snowmelt*)	Melting snow measured as a negative change in *SWE* at a SNOTEL station.	cm day^{-1}
Daily Air Temperature (*Air Temp.*)	Average daily air temperature across the watershed from PRISM.	°C

Period	Description
Water year	Water Year, October 1st through September 30th, period used in the U.S. to reflect water management practices (Pagano et al. 2009).
Low-flow	October 1st to start of spring runoff represents period during which streamflow is primarily composed of baseflow (Miller et al. 2014).
High-flow	Start of spring runoff to October 1st, represents period during which streamflow is composed of flow from spring runoff and the corresponding recession (Rumsey, Miller, and Sexstone 2020).
Melt	Peak *SWE* to melt out, period over which most snowfall melts in a water year (Hammond, Saavedra, and Kampf 2018).
Runoff	Start of spring runoff to date of highest peak flow, period over which streamflow increases due to snowmelt (Rumsey, Miller, and Sexstone 2020).
Recession	Date of highest peak flow to October 1st, period over which streamflow generally declines to lack of significant precipitation (Barnhart et al. 2016).
Winter	October 1st through date of peak *SWE*, period over which most of the watershed's precipitation falls as snow (Wolf et al. 2023).

Cayan, and Dettinger 2004). Rain is a larger fraction of total precipitation at lower elevations in the West (Ficklin, Robeson, and Knouft 2016; Hammond et al. 2019; Knowles, Dettinger, and Cayan 2006). As climate change has caused warmer winter temperatures, the amount of snowmelt occurring during winter has increased and could affect streamflow (Harpold and Brooks 2018; Marshall et al. 2020; Sexstone et al. 2018). In some cases, snowmelt rate is a better predictor of streamflow in the western US compared to snowfall or rainfall (Barnhart et al. 2016; Rumsey, Miller, and Sexstone 2020; Wolf et al. 2023).

The precipitation input to watersheds following spring snowmelt is predominantly rainfall in the western US (Bales et al. 2006; Dettinger, Udall, and Georgakakos 2015; Ficklin, Robeson, and Knouft 2016; Hammond et al. 2019). Significant amounts of summer and fall rain could cause changes in baseflow contributions during the *low-flow* period (Hammond et al. 2019; Knowles, Dettinger, and Cayan 2006). The rate of streamflow increase during the *runoff* period potentially represents both the storage condition of the aquifer(s) in the watershed and the snowmelt rate (Bales et al. 2006; Barnhart, Tague, and Molotch 2020; Brooks et al. 2015, 2021; Godsey, Kirchner, and Tague 2014). The recession rate captures the storage condition of the aquifer(s) in the watershed post-spring runoff and the impact of any significant precipitation events on the aquifer(s) storage condition post-snowmelt (Brooks et al. 2021; Godsey, Kirchner, and Tague 2014; Liu, Williams, and Caine 2004; Liu et al. 2008).

To represent all the potential relationships described above, and provide a robust variable pool of all variables potentially predictive of streamflow regimes, the minimum (*MIN*), maximum (*MAX*), average (*AVG*), cumulative-total (*TOTAL*), and average daily change (*ΔAVG*) in each hydrological characteristic metric was calculated for each hydrologic period (Table 1) (Addor et al. 2018; McMillan 2021). In this paper, variables are denoted by the metric (*q*, *PRCPSA*, *SWE*, *Rain*, etc.), a subscript representing the measured hydrologic period (*low-flow*, *high-flow*, *runoff*, etc.), a subscript representing the sampling statistic (*AVG*, *MIN*, etc.), and final subscript of *WY* or *WY-1* denoting whether the variable measurement period occurs in the same water year as the response variable in the MLR equations or the prior water year, respectively. A generic variable would be written as $Metric_{hydrologic\ period,\ sampling\ statistic,\ WY\ or\ WY\text{-}1}$. A complete list of variables used in the MLR analysis of $q_{low\text{-}flow,\ TOTAL,\ WY}$ and $q_{high\text{-}flow,\ TOTAL,\ WY}$ are provided (Tables S3 and S4).

2.4 | Watershed Hydrologic Regime Characteristics

We compared distributions across water years of certain key metrics and characteristic ratios to discern any clear differences or similarities among the hydrologic patterns of the examined watersheds. Additionally, the hydrograph time series were examined for trends in streamflow during *high-flow* and *low-flow* in response to water year precipitation changes using a simple linear regression.

The distributions of $Precip_{water\ year,\ TOTAL,\ WY}$, $q_{water\ year,\ TOTAL,\ WY}$, $q_{high\text{-}flow,\ TOTAL,\ WY}$, and the $q_{low\text{-}flow,\ TOTAL,\ WY}$, were compared between watersheds. The snow fraction, runoff ratio, $q_{low\text{-}flow,\ TOTAL,\ WY}$ to $q_{water\ year,\ TOTAL,\ WY}$ ratio, and $q_{low\text{-}flow,\ TOTAL,\ WY}$ to $q_{high\text{-}flow,\ TOTAL,\ WY}$ ratio were calculated for each watershed (Equations 1–4, respectively).

$$\text{snow fraction} = \frac{\text{Snow}_{\text{water year, TOTAL, WY}}}{\text{PRCPSA}_{\text{water year, TOTAL, WY}}} \tag{1}$$

$$\text{runoff ratio} = \frac{q_{\text{water year, TOTAL, WY}}}{\text{Precip}_{\text{water year, TOTAL, WY}}} \tag{2}$$

$$\text{low} - \text{flow ratio} = \frac{q_{\text{low–flow, TOTAL, WY}}}{q_{\text{water year, TOTAL, WY}}} \tag{3}$$

$$\text{low} - \text{flow to high} - \text{flow ratio} = \frac{q_{\text{low–flow, TOTAL, WY}}}{q_{\text{high–flow, TOTAL, WY}}} \tag{4}$$

2.5 | Multi-Linear Regression (MLR) Analysis

MLR models using different hydrological variables are often used to produce streamflow forecasts and determine variable correlations with streamflow. These hydrological variables represent different watershed processes in streamflow generation (Fleming and Goodbody 2019; Vogel, Wilson, and Daly 1999). One of the most used MLR modelling frameworks is the monthly water supply forecast produced by the NRCS using SNOTEL snowpack and climate data and USGS streamflow data. Using MLR, significant variables are selected from a wide range of measured and calculated metrics across different periods for a stream gage. Identified variables are used in an MLR equation to predict streamflow at a monthly time scale (Garen 1992).

In this study, we use a methodology similar to that outlined in Garen (1992) to select variables from the variable pools (Tables S3 and S4) most related to and predictive of the total streamflow volume during the *low-flow* period of a water year ($q_{low\text{-}flow,\ TOTAL,\ WY}$) and the total streamflow volume during the *high-flow* period of a water year ($q_{high\text{-}flow,\ TOTAL,\ WY}$). For each variable in the variable pool, a linear regression was completed and a *t*-test (p-value ≤ 0.05) was used to determine if the variable was significantly associated with the response variable, $q_{low\text{-}flow,\ TOTAL,\ WY}$ or $q_{high\text{-}flow,\ TOTAL,\ WY}$.

For each possible variable pair combination in the respective variable pools, an MLR equation was established with the following form:

$$q_{x\text{–flow, TOTAL, WY}} = C_1 V_1 + C_2 V_2 + b \tag{5}$$

where the subscript x refers to low or high flow, C_1 and C_2 are regression coefficients, V_1 and V_2 are variables in every possible pair in Tables S3 and S4, and b is the regression intercept. If the regression coefficients of each variable passed a *t*-test (p-value ≤ 0.05), the MLR equation using the variable pair was considered potentially viable. If the sign of the coefficients in the linear regression of both variables in the variable pair matched the sign of the coefficient of each respective variable in the MLR equation, then the MLR equation using the variable pair was then considered viable. Once a list of viable equations of $q_{low\text{-}flow,\ TOTAL,\ WY}$ and $q_{high\text{-}flow,\ TOTAL,\ WY}$ were created, the r^2 values for each equation were calculated by comparing predicted values of $q_{low\text{-}flow,\ TOTAL,\ WY}$ and $q_{high\text{-}flow,\ TOTAL,\ WY}$

to observed values during the respective periods. The r^2 values were then used to rank the equations. The top 10% of equations were selected and trends in the metrics and periods of variables used in MLR equations explaining the highest r^2 and proportional variance were then examined for this subset of equations. While the best-fit equation was identified for $q_{low\text{-}flow,\ TOTAL,\ WY}$ and $q_{high\text{-}flow,\ TOTAL,\ WY}$ in each watershed, the best predictive equations were also determined by restricting variables used in the regressions to those occurring in hydrological periods prior to the measurement period of the response variable (Tables S3 and S4).

3 | Results

Examination and comparison of the relationship of the different hydrologic characteristic metrics with $q_{low\text{-}flow,\ TOTAL,\ WY}$ and $q_{high\text{-}flow,\ TOTAL,\ WY}$ indicates some consistencies and differences between the karst and non-karst watersheds in this study. Analysis of the MLR equations further reveals differences between karst and non-karst watersheds in the characteristic metrics related to and predictive of $q_{low\text{-}flow,\ TOTAL,\ WY}$.

3.1 | Watershed Hydrologic Regime Characteristics

We examine the distribution of important variables to understand the variability in our key hydrologic metrics of interest (q and *Precip.*). The $Precip_{water\ year,\ TOTAL}$, $q_{water year,\ TOTAL}$, $q_{high\text{-}flow,\ TOTAL}$, and $q_{low\text{-}flow,\ TOTAL}$ distributions for each watershed are used to calculate snow fraction, runoff ratio, $q_{low\text{-}flow,\ TOTAL}/q_{water\ year,\ TOTAL}$, and $q_{low\text{-}flow,\ TOTAL}/q_{high\text{-}flow,\ TOTAL}$ distributions across the period of record (Figure 3). The differences between karst and non-karst watersheds are apparent. The $Precip_{water\ year,\ TOTAL}$ is relatively consistent between watersheds while the mean $PRCPSA_{water\ year,\ TOTAL}$ differs across watersheds (Figure 3 and Table S5). This can be attributed to the SNOTEL stations only representing a point in each watershed and elevation differences between the SNOTEL stations.

Based on similar *Precip.*, we expect the watersheds to have a similar $q_{water\ year,\ TOTAL}$ magnitude, however, that is not always the case. The distributions of $q_{water\ year,\ TOTAL}$ are similar in the Logan River, American Fork, Weber River, Bear River-Stillwater Fork, and Lake Fork (Figure 3 and Table S5). Red Butte Creek and the Blacksmith Fork have narrow distributions with a lower range compared to the other watersheds (Figure 3 and Table S5). The $q_{water\ year,\ TOTAL}$ distribution in all watersheds is skewed towards larger values.

The $q_{high\text{-}flow,\ TOTAL}$ distributions across all seven watersheds exhibit a similar pattern to the $q_{water\ year,\ TOTAL}$ distributions (Figure 3 and Table S5). This is likely due to most of the $q_{water\ year,\ TOTAL}$ being concentrated during the *high-flow* period. This is expected behaviour in snow-dominated watersheds. The pattern in comparing the $q_{low\text{-}flow,\ TOTAL}$ distributions across watersheds is also similar to the $q_{water\ year,\ TOTAL}$ distribution with the significant difference being the $q_{low\text{-}flow,\ TOTAL}$ distribution ranges are significantly smaller (Figure 3 and Table S5). The snow fraction distributions have a median value above 0.5 with overlapping distribution ranges, confirming that all the watersheds in the study experience snow-dominated precipitation regimes (Figure 3 and Table S5).

The median runoff ratios in the karst watersheds (Logan River, Red Butte Creek, American Fork, and Blacksmith Fork) are all lower than those in the non-karst watersheds (Weber River, Bear River, and Lake Fork). The Logan River and American Fork median runoff ratios are slightly higher at approximately 0.35, whereas Red Butte Creek and Blacksmith Fork have medians of approximately 0.2. The median runoff ratios in the non-karst watersheds are all around 0.5 (Figure 3 and Table S5). The runoff ratios would indicate that a larger fraction of precipitation is lost (to deeper groundwater systems or ET) or stored in the karst watershed aquifers compared to the non-karst watersheds. Additionally, inter-basin movement of groundwater through karst aquifers that cross watershed topographic boundaries has been documented to some extent by Spangler (2001) in the Logan River watershed; however, inter-basin transfer has not been explored in these watersheds despite it being a common feature of karst watersheds (Pulido-Bosch 2021; Winter 1995).

The $q_{low\text{-}flow,\ TOTAL}/q_{water\ year,\ TOTAL}$ distributions show that the ratio in karst watersheds is on average higher than that in non-karst watersheds, with notably high median values of approximately 0.3 in the Logan River and Blacksmith Fork (Figure 3 and Table S5). The $q_{low\text{-}flow,\ TOTAL}/q_{high\text{-}flow,\ TOTAL}$ distributions again show higher medians for the karst watersheds when compared to the non-karst watersheds (Figure 3 and Table S5). With the karst watersheds showing both significantly higher medians and wider ranges in their distributions, this suggests the presence of large aquifers with significant storage capacity as discussed in Iliopoulou et al. (2019).

Collectively, these ratios indicate that there are differences between the karst and non-karst watersheds, especially concerning the significant fraction of $q_{water\ year,\ TOTAL}$ that is observed during the *low-flow* period in karst watersheds (Figure 3). This suggests that baseflow periods differ between karst and non-karst watersheds.

3.2 | Time Series Trends

The difference in streamflow observed during the *low-flow* period in the karst watersheds compared to the non-karst watersheds is further demonstrated by comparing the hydrograph of a karst (Logan River) to a non-karst (Bear River-Stillwater Fork) watershed (Figure 4). First, we observed that the precipitation patterns, measured as *Snowmelt* plus *Rain* at the SNOTEL stations within the respective watersheds, showed similar trends over the period of record, while magnitudes differed between the two watersheds (Figure 4a,b). Here we use SNOTEL *Snowmelt* and *Rain* instead of PRISM *Precip.* because we can differentiate between *Snowmelt* and *Rain*. Comparison of the SNOTEL *PRCPSA* and PRISM *Precip.* data show good agreement with respect to the time-series trends and the distributions are similar across watersheds (Figure 3, Table S5). Second, the streamflow in both watersheds is responsive to precipitation, with the minimum *low-flow* and maximum *high-flow* streamflow increasing and decreasing relative to cumulative *Snowmelt* plus *Rain* on a water year basis (Figure 4a,b). Next, we see that the karst-dominated Logan River minimum and maximum average streamflow

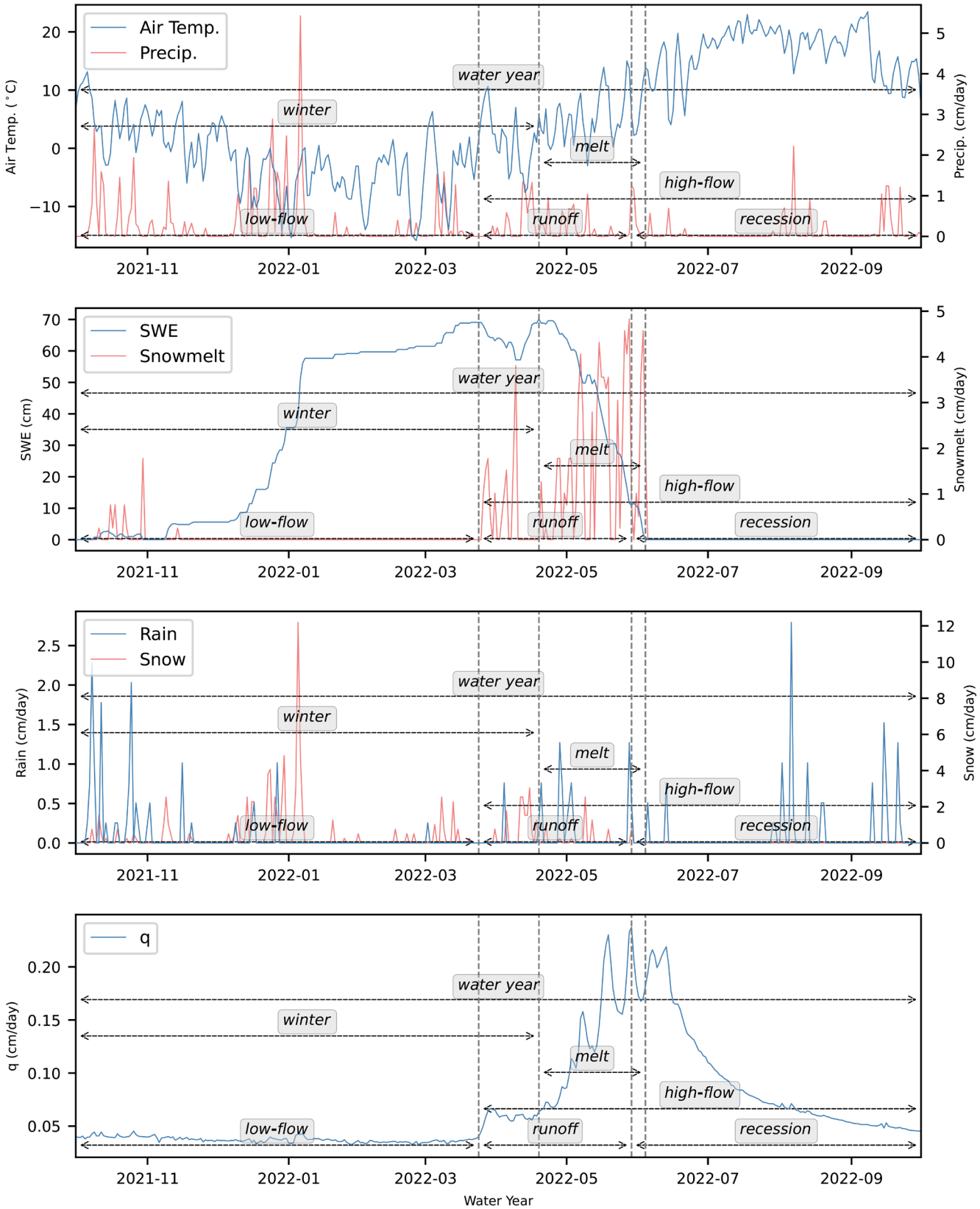

FIGURE 2 | Hydrological periods denoted by the labelled arrows defined for hydrologic metrics described in Table 1.

for the *low-flow* period occupies a wider and higher range (0.03–0.09 cm day^{-1}) when compared to the non-karst Bear River-Stillwater Fork (0.02–0.05 cm day^{-1}) (Figure 4a,b). The Logan River streamflow during *low-flow* exhibits a lagged response to changes in precipitation as exhibited in the 2017–2021 water years. In contrast, the Bear River-Stillwater Fork shows a return to a consistent streamflow during *low-flow* with some variability due to fall precipitation events.

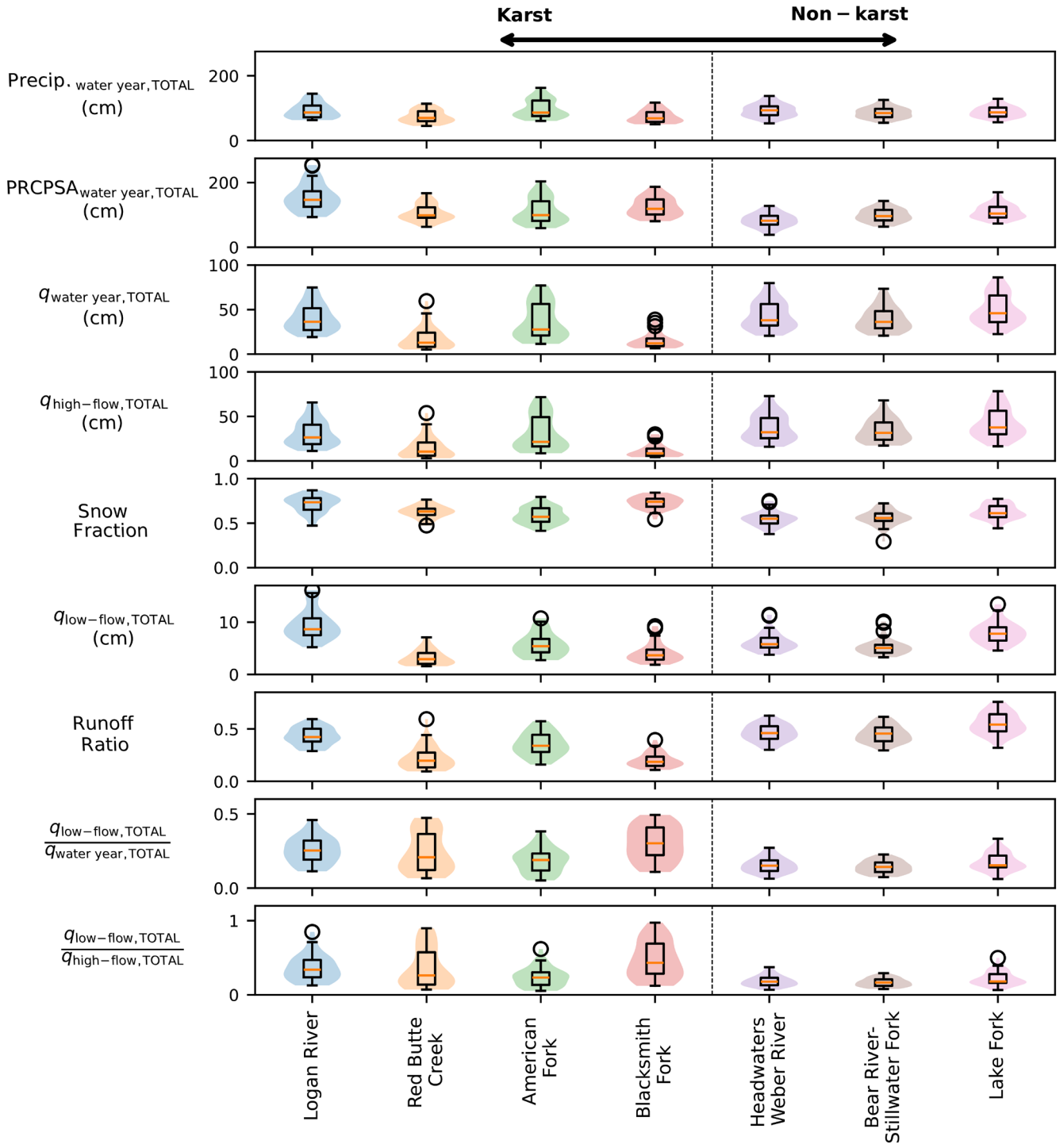

FIGURE 3 | Watershed characteristic comparisons. The boxplot distribution is overlaid by a violin plot of the distribution of values for each watershed. Watersheds are ordered from left to right based on percentage of carbonate rock area.

Notably, we observe a significant spike in streamflow late in the 2021 water year due to above-average rain in the Bear River-Stillwater Fork, while no apparent spike appears in the Logan River streamflow resulting from these same events (Figure 4c,d). The streamflow during *high-flow* appears to be bolstered in below median *Snowmelt* plus *Rain* years by the long recession of flows occurring in karst systems following above median *Snowmelt* plus *Rain* years as observed in the 2017–2018 water years in Figure 4c. This pattern appears in hydrographs of all the karst watersheds (Figures S1–S3).

Similar hydrograph trends and differences are observed when comparing the karst and non-karst hydrographs of the other watersheds in this study (Figures S1–S5). A lack of response to rain events in the karst watersheds is likely due to the interception of any overland flow by fractures, caves and sinkholes. In contrast, the fast response in non-karst watersheds can be attributed to overland flow or shorter subsurface storm flow paths.

Simple regression of the $Precip_{water\ year,\ TOTAL,\ WY}$ against $q_{water\ year,\ TOTAL,\ WY}$, $q_{high\text{-}flow,\ TOTAL,\ WY}$, and $q_{low\text{-}flow,\ TOTAL,\ WY+1}$

supports what we observed in the hydrograph time series (Figure 5). Both karst and non-karst watersheds show a strong correlation between $q_{wateryear, TOTAL, WY}$ and $Precip_{wateryear, TOTAL, WY}$ (Figure 5) as demonstrated in watersheds across the West (Dierauer, Whitfield, and Allen 2018; Knowles, Dettinger, and Cayan 2006). Notably, across all watersheds the r^2 is higher between $q_{high\text{-}flow, TOTAL, WY}$ and $Precip_{water\ year, TOTAL, WY}$ (Figure 5). This is not surprising given that streamflow during the *high-flow* period is driven by snowmelt, which in these snow-dominated watersheds represents a majority of the accumulated *Precip.* in a water year. When comparing the $q_{low\text{-}flow, TOTAL, WY+1}$ to $Precip_{water\ year, TOTAL, WY}$, in the karst watersheds the r^2 values are higher compared to the non-karst watersheds (Figure 5). This indicates a stronger correlation between snowpack and *low-flow* volumes in karst watersheds than in the non-karst watersheds. This would be indicative of the responsive nature of karst aquifers to annual snowpack and the karst aquifer connection to streamflow during the *low-flow* period.

3.3 | Low-Flow Relationships

In both the karst and non-karst watersheds, MLR equations using variables containing streamflow, *q*, sampled within the *winter* or *high-flow* periods had a relatively good fit to the data with r^2 values ranging from 0.57 to 0.97 (Figures 6 and 7 and Table S6). In the Logan River, Red Butte Creek, American Fork, and Blacksmith Fork, the equation with the highest r^2 contains the variable *q* (Figure 6 and Table S6). $q_{recession, MIN, WY\text{-}1}$, the lowest streamflow value during the *recession* period prior to the start of the *low-flow* period, alone is a good predictor as measured by r^2 in the karst watersheds, but is a relatively poor predictor on its own in the non-karst watersheds. The best MLR equations for the non-karst watersheds overall have weaker r^2 values when compared to the best MLR equations for the karst watersheds (Figures 6 and 7 and Table S6).

In the non-karst watersheds, metrics measuring *q*, *Snowmelt* and *Air Temp.*, appeared in equations highly correlated with $q_{low\text{-}flow, TOTAL, WY}$. While the *q* variable appears in the equations most correlated with $q_{low\text{-}flow, TOTAL, WY}$ in every watershed, in the karst watersheds nearly all the proportional variance is explained by the streamflow, *q*, variable (Figure 8 and S6–S8). In contrast, in the non-karst watersheds, the proportional variance explained by any given variable is balanced across metrics including *q*, *Precip.*, *Snowmelt*, and *Air Temp.*, indicating complex processes driving $q_{low\text{-}flow, TOTAL, WY}$ in non-karst watersheds (Figures S9–S11).

3.4 | Low-Flow Predictive Equations

The list of viable MLR equations was restricted to those based on variable pairs containing variables sampled over periods prior to the *low-flow* period, resulting in a list of predictive equations useful in a management or planning context. The best predictive equations in the karst watersheds have r^2 values ranging from 0.77 to 0.92 with $q_{WY\text{-}1}$ being the most common regression variable explaining a majority of the variance in the predicted results of $q_{low\text{-}flow, TOTAL, WY}$ (Table 2 and Figure S12). These results, in combination with the highest ranked MLR regression results, indicate that in the karst watersheds, past streamflow is a good indicator of future streamflow.

In the Weber River and Bear River, $q_{low\text{-}flow, TOTAL, WY\text{-}1}$ and $q_{winter, TOTAL, WY\text{-}1}$ explain a significant amount of the proportional variance in predicted results; however, the r^2 values produced by the equations, 0.66 and 0.65, respectively, show that the equations are not useful for predicting $q_{low\text{-}flow, TOTAL, WY}$ (Table 2, Figure S13). In the prediction equations for $q_{low\text{-}flow, TOTAL, WY}$ in Lake Fork, *Snowmelt* produces the best predictive MLR equation with an r^2 value of 0.34. In general, the lack of predictive power of the equations in the non-karst watersheds indicates that the *low-flow* regimes are less dependent on prior hydrologic conditions characterised by individual metrics and instead require models that capture more complex hydrologic processes (Table 2).

3.5 | High-Flow Relationships

Using all variable pair combinations, MLR analysis allows for the determination of the strength of variable relationships with $q_{high\text{-}flow, TOTAL, WY}$. The variable pairs and the results for the top 10% of the viable MLR equations highlight the importance of precipitation via the strong relationship between *Precip.*, *Snow*, *Rain*, *SWE*, and *Snowmelt*, and $q_{high\text{-}flow, TOTAL, WY}$. It is not surprising that r^2 values range from 0.90 to 0.94 (Figures 9 and 10), given the well-documented relationship between snowpack and peak streamflow in western snowmelt-dominated watersheds (Barnhart, Tague, and Molotch 2020; Brooks et al. 2021; Rumsey, Miller, and Sexstone 2020).

In all of the watersheds, the metrics best related to $q_{high\text{-}flow, TOTAL, WY}$ are measures of precipitation (*Precip.*, *SWE*, and *Snowmelt*) during the *Winter* or *low-flow* periods (Figures 11 and S14–S19). In all watersheds, $SWE_{high\text{-}flow, AVG, WY}$ is a reasonably good predictor because snow is the dominant precipitation source.

3.6 | High-Flow Predictive Equations

The metrics appearing in the best $q_{high\text{-}flow, TOTAL, WY}$ prediction equations are similar to those metrics in the MLR equations with the strongest relationship with $q_{high\text{-}flow, TOTAL, WY}$. *Precip.* and *SWE* are the most common metrics explaining a significant portion of the variance in prediction results with r^2 values ranging from 0.77 to 0.84 (Table 3). The best predictive variables are metrics representing different forms of precipitation measured during the *low-flow* period (Figures 10 and S14–S19). This is consistent with our understanding of the influence of the snowpack on the *high-flow* regime in western snowmelt-dominated watersheds. Generally, the predictive equations provide acceptable results in all watersheds (Figures S20 and S21).

4 | Discussion

Streamflow volumes are closely related to storage conditions in a watershed (Brooks et al. 2021; Godsey, Kirchner,

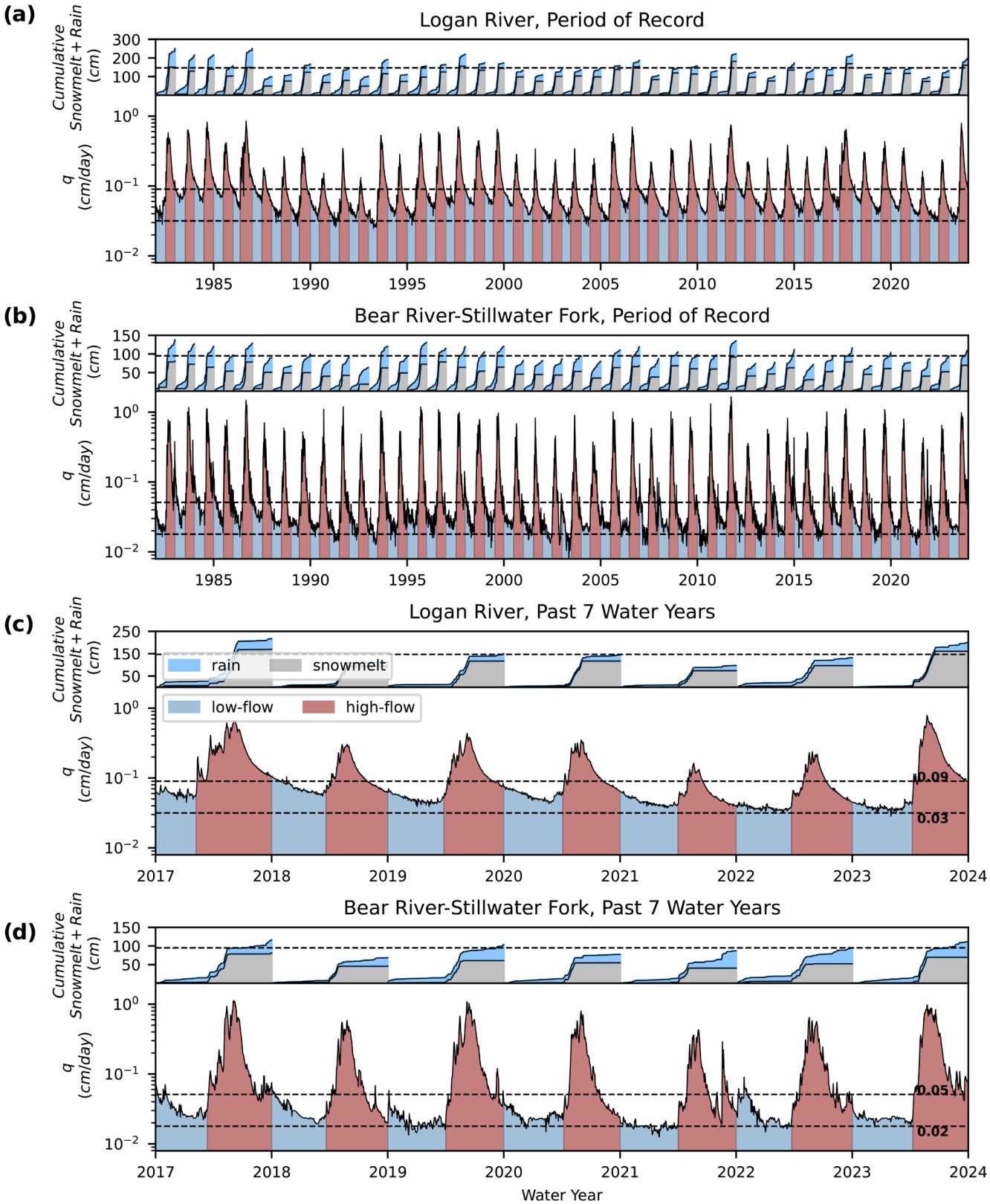

FIGURE 4 | Cumulative *Snowmelt + Rain* and daily *q* for the period of record (a, b) for the Logan River and Bear River-Stillwater Fork, respectively. Cumulative *Snowmelt + Rain* and daily streamflow, *q*, for the 2017 through the 2023 water year (c, d) for the Logan River and Bear River-Stillwater Fork, respectively. Horizontal dashed lines in the *Snowmelt + Rain* plots show the median *Snowmelt + Rain* for the period of record for the respective watershed, while horizontal dashed lines in the streamflow plots show the minimum and maximum $q_{low\text{-}flow,\ AVG,\ WY}$ values.

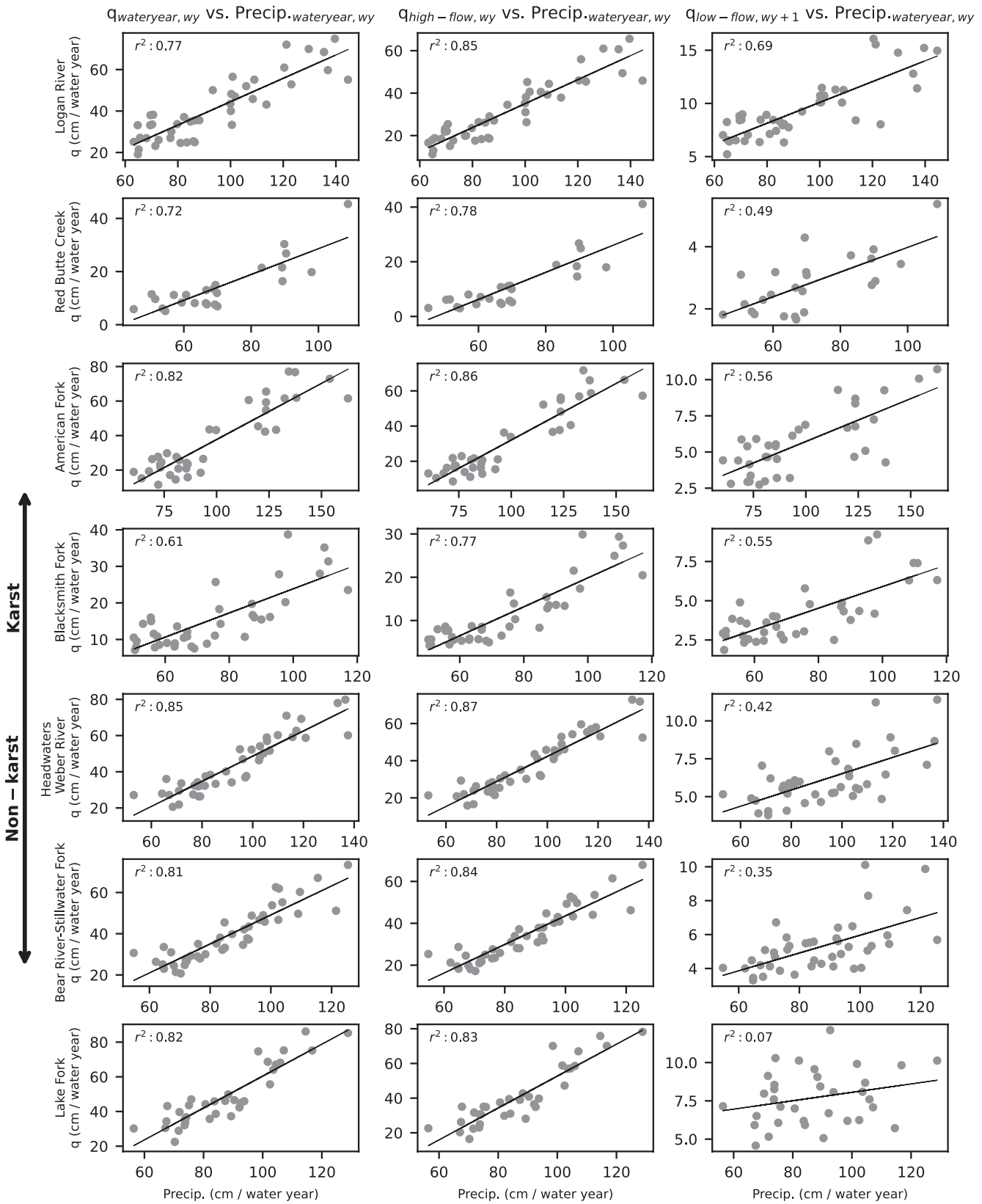

FIGURE 5 | Area normalised streamflow totaled for the water year (first column), the *high-flow* period (second column), and the *low-flow* period (third column) plotted against total water year precipitation for each watershed (rows).

and Tague 2014). While most streamflow in snow-dominated watersheds is produced during spring runoff, the dominant source during fall and winter is groundwater storage (Cochand et al. 2019; Land and Timmons 2016; Rumsey, Miller, and Sexstone 2020). Variations in post-runoff streamflow within different non-karst watersheds have been attributed to variations

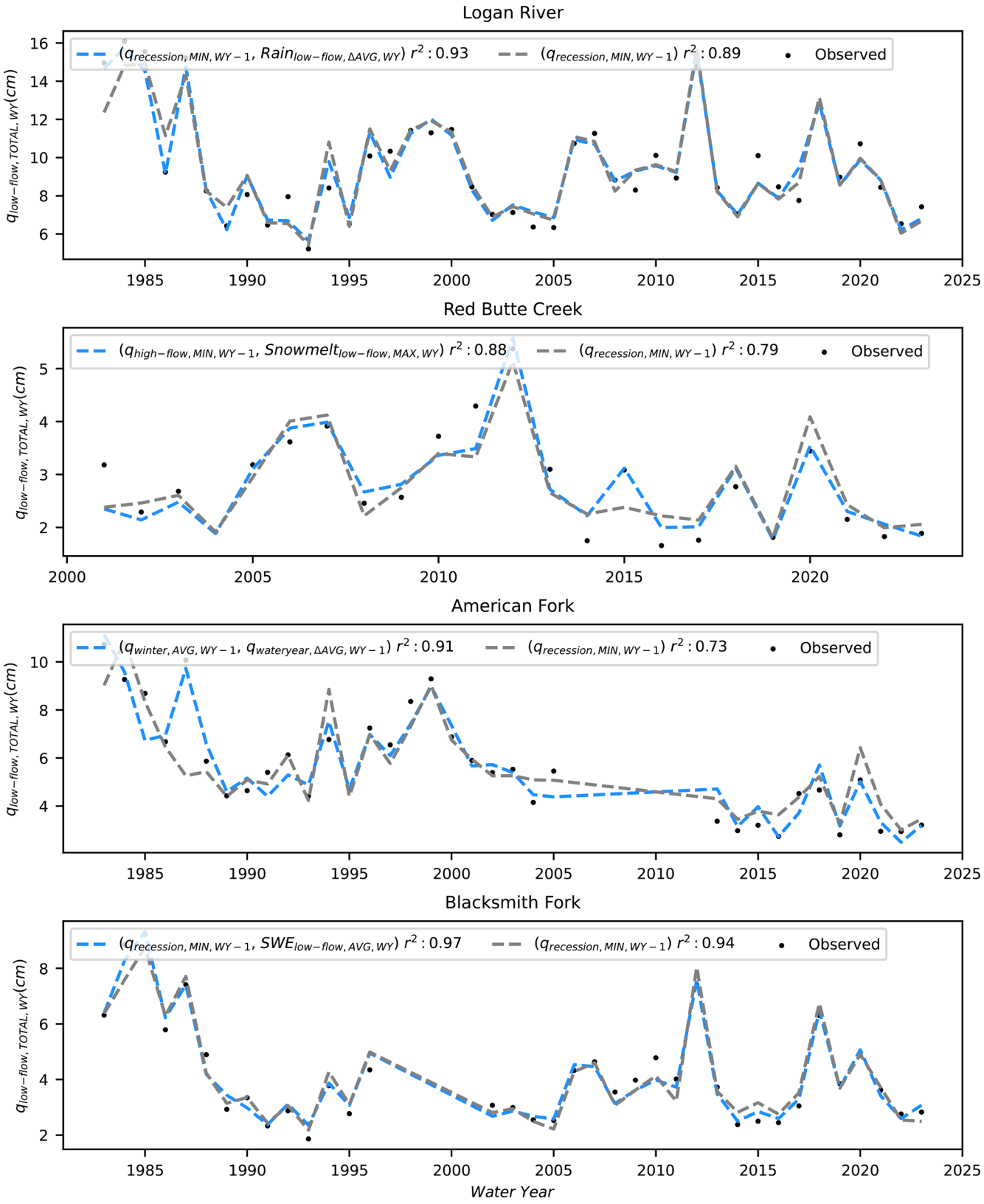

FIGURE 6 | $q_{low\text{-}flow,\ TOTAL,\ WY}$ regression results for the karst watersheds. The blue dashed line shows the results for the highest rank MLR equation and the associated variable pair. The grey dotted line shows the regression results for $q_{recession,\ MIN,\ WY\text{-}1}$. The observed $q_{low\text{-}flow,\ TOTAL,\ WY}$ values are shown by the black dots.

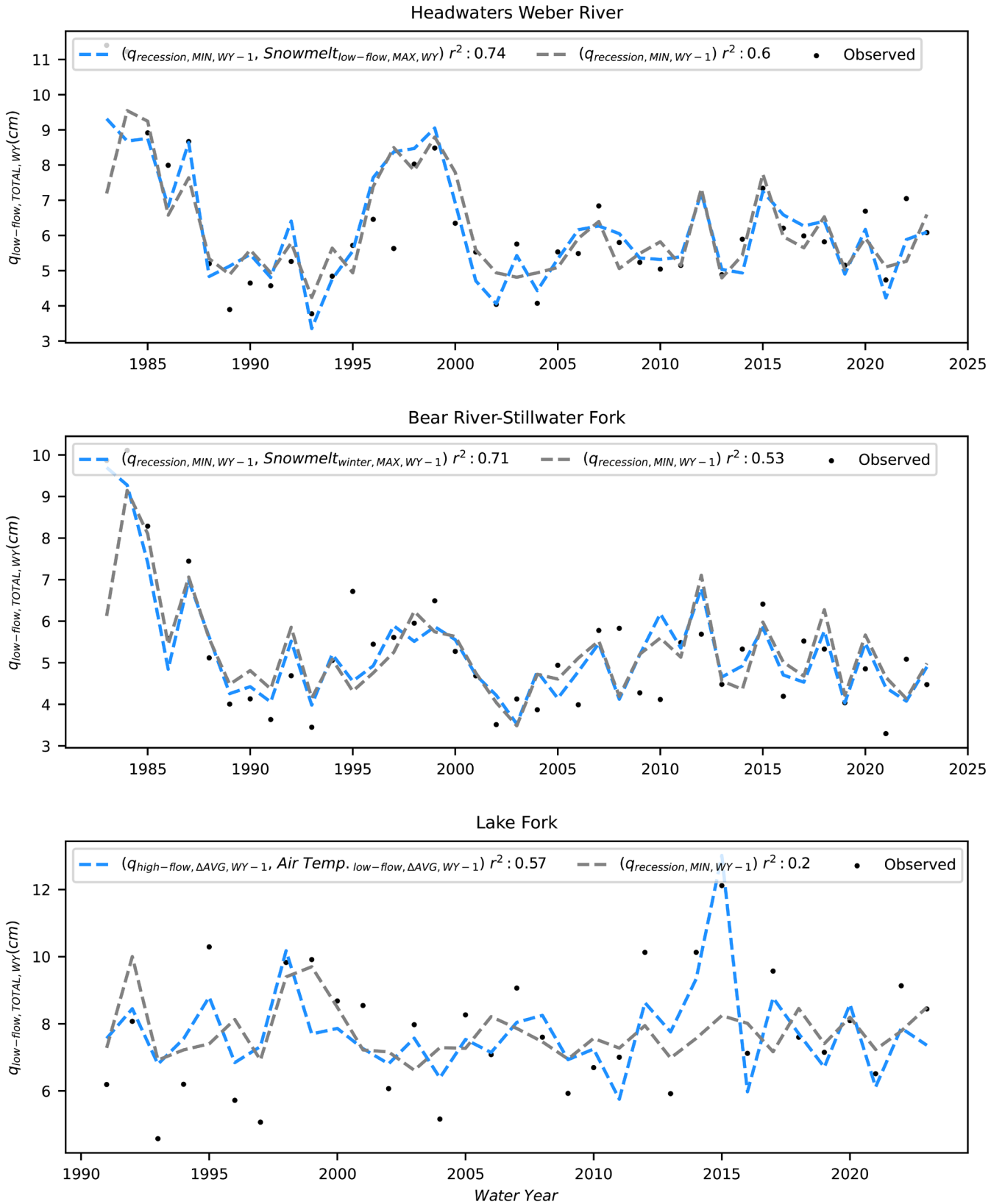

FIGURE 7 | $q_{low\text{-}flow,\,TOTAL,\,WY}$ regression results for the non-karst watersheds. The blue dashed line shows the results for the highest rank MLR equation and the associated variable pair. The grey dotted line shows the regression results for $q_{recession,\,MIN,\,WY\text{-}1}$. The observed $q_{low\text{-}flow,\,TOTAL,\,WY}$ values are shown by the black dots.

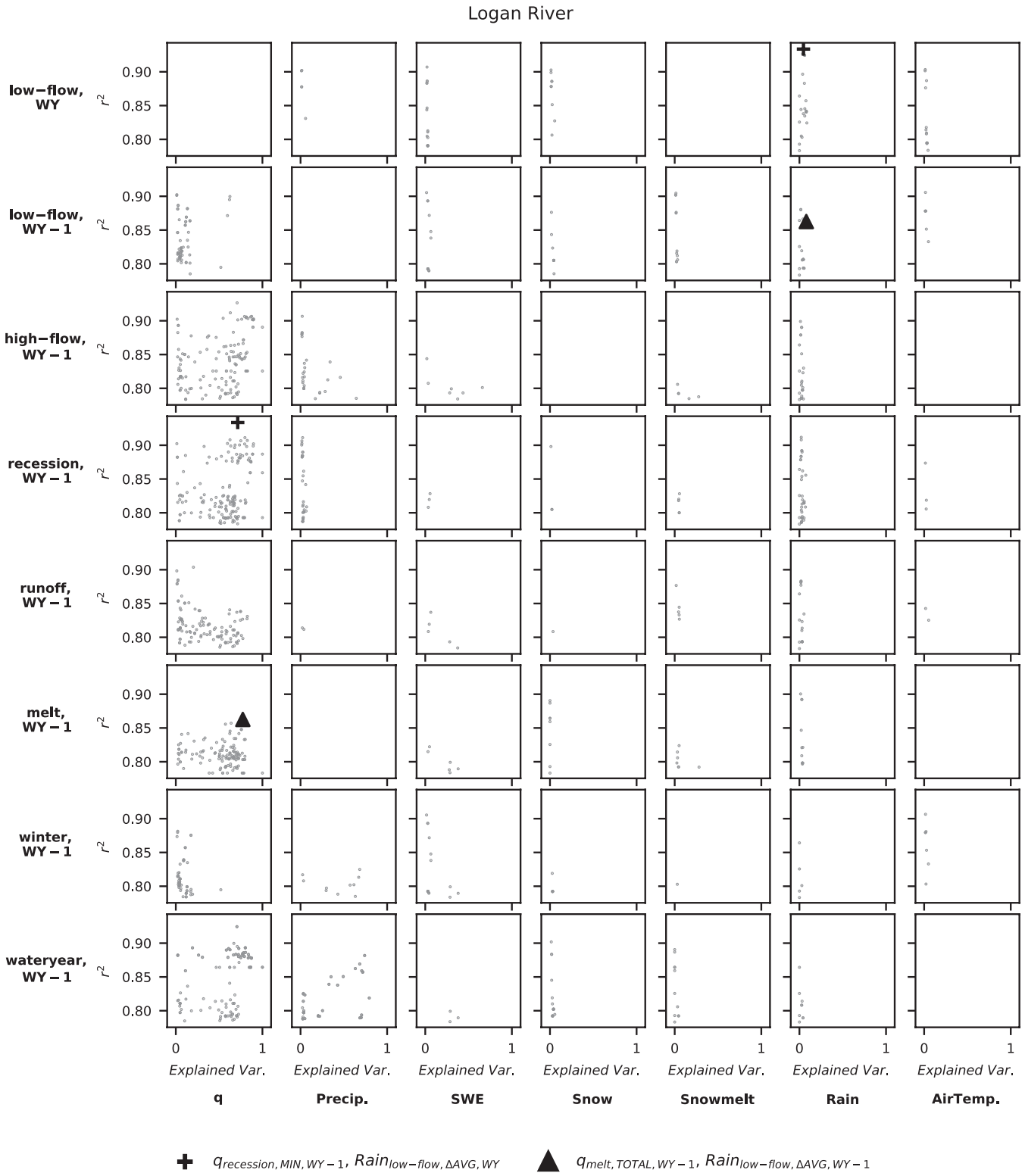

FIGURE 8 | Logan River, MLR equation variables' relationship strength to $q_{low\text{-}flow,\ TOTAL,\ WY}$. Each column of plots represents a different metric, and each row represents a different hydrologic period used in the MLR analysis. Corresponding variables in the top 10% of viable MLR equations are represented in each plot. A plot's y-axis represents the r^2 value of an equation while the x-axis denotes the fraction of explained proportional variance by a given equation variable. The variable pair from the highest ranked equation is represented by "+" s (Figure 6) and variables from the best prediction equation are shown by triangles (Table 2). Variables in all other MLR equations are represented as grey dots.

in storage, however, contributions are often variable due to changes in rainfall (Kirchner 2016; McNamara et al. 2011). The larger storage volume of karst watersheds is a complicating factor in understanding streamflow regimes due to the complex and heterogeneous distribution of storage and flow paths in these watersheds (Pulido-Bosch 2021; Spangler 2001; Thurber

TABLE 2 | Best low-flow prediction equations for the study watersheds of the form $q_{low\text{-}flow,\ TOTAL,\ WY} = C_1 \times V_1 + C_2 \times V_2 + b$.

Watershed	Coefficient 1 (C_1)	Variable 1 (V_1)	Coefficient 2 (C_2)	Variable 2 (V_1)	Intercept (b)	r^2	RMSE
Logan River (karst)	0.303	$q_{melt,\ TOTAL,\ WY\text{-}1}$	−244.70	$Rain_{low\text{-}flow,\ \Delta AVG,\ WY\text{-}1}$	5.278	0.86	1.02
Red Butte Creek (karst)	12.70	$q_{runoff,\ AVG,\ WY\text{-}1}$	0.463	$Snowmelt_{winter,\ MAX,\ WY\text{-}1}$	1.417	0.77	0.45
American Fork (karst)	91.10	$q_{runoff,\ MIN,\ WY\text{-}1}$	0.227	$q_{melt,\ TOTAL,\ WY\text{-}1}$	1.142	0.84	0.88
Blacksmith Fork (karst)	21.27	$q_{melt,\ AVG,\ WY\text{-}1}$	30.10	$q_{winter,\ AVG,\ WY\text{-}1}$	1.373	0.92	0.52
Headwaters Weber River (non-karst)	0.446	$q_{low\text{-}flow,\ TOTAL,\ WY\text{-}1}$	0.0746	$Precip_{low\text{-}flow,\ TOTAL,\ WY\text{-}1}$	−0.4170	0.66	1.00
Bear River-Stillwater Fork (non-karst)	0.457	$q_{winter,\ TOTAL,\ WY\text{-}1}$	0.526	$Snowmelt_{winter,\ MAX,\ WY\text{-}1}$	2.094	0.65	0.87
Lake Fork (non-karst)	−614.6	$Snowmelt_{winter,\ \Delta AVG,\ WY\text{-}1}$	0.0594	$Snowmelt_{runoff,\ TOTAL,\ WY\text{-}1}$	5.365	0.34	1.43

et al. 2024). Karst watersheds are particularly vulnerable to changes in storage as a large fraction of year-round streamflow is derived from groundwater (Liu, Wagener, and Hartmann 2021; Neilson et al. 2018). This is of particular concern since karst systems supply water to 20%–25% of the world's population (Ford and Williams 2013; Hartmann et al. 2014). The connection between karst aquifers and streamflow regimes is a growing concern globally and in the western US as climate change shifts precipitation regimes and karst water resources are threatened (Dieter et al. 2018; Donovan et al. 2022; Segura et al. 2019; Tobin et al. 2018).

The presence of karst storage shifts the streamflow distribution between the *high-flow* and *low-flow* periods as indicated by the $q_{low\text{-}flow,\ TOTAL}/q_{high\text{-}flow,\ TOTAL}$ and the $q_{low\text{-}flow,\ TOTAL}/q_{water\ year,\ TOTAL}$ of the analysed watersheds (Figure 3). This shift in distribution manifests as a longer recession tail and reduced peak flow when comparing karst to non-karst watersheds, respectively (Figures 4 and S1–S5). The hydrographs of the karst watersheds highlight the presence of a "memory effect" (Fiorillo 2009, 2014; Hosseini, Ataie-Ashtiani, and Simmons 2017; Mangin 1984) where streamflow in water years experiencing below median precipitation was bolstered by flows from karst storage banked during previous years of high precipitation. This memory effect was investigated using time series lag analysis to see if a persistent lag-period could be determined, however, no constant period was significantly predictive of future streamflow volume. The tangible consequence of this memory effect for water managers and users in karst watersheds is higher low flows during short drought periods, but the longevity of elevated baseflow is highly dependent on the annual recharge quantities. Regardless, within a water year, the stable recession curves can result in a predictable amount of water available during critical, low-flow periods. In contrast, in the non-karst watersheds prior streamflow was a weak predictor of $q_{low\text{-}flow,\ TOTAL,\ WY}$ (Figures S9–S11). The metrics explaining the most variance in the prediction of $q_{low\text{-}flow,\ TOTAL,\ WY}$ are varied and still result in poor predictions, indicating complex hydrologic processes in the non-karst watersheds (Figures S9–S11).

Low-flow volume, $q_{low\text{-}flow,\ TOTAL,WY}$ can accurately be anticipated by the predictive equations in karst watersheds (Table 2). *Low-flow* volumes are most strongly related to *recession* streamflow volumes, $q_{recession,\ MIN,\ WY\text{-}1}$ (Figures 8 and S6–S8). Various measures of precipitation are strongly related to *high-flow* volumes (Figures 11 and S14–S19, and Tables 3 and S7), as expected due to the high snow fraction in these watersheds (Figure 3). Taken together, this indicates the storage condition is significantly affected by yearly snowpack. Examination of the karst watershed hydrographs (Figures 4 and S1–S3) and distribution of the $q_{low\text{-}flow,\ TOTAL}/q_{high\text{-}flow,\ TOTAL}$ (Figure 3) once again illustrates that the karst watersheds experience the memory effect to different degrees. As discussed by Thurber et al. (2024), karst aquifers can exhibit varying levels of connectivity to rivers. The Logan River and Red Butte Creek appear well-connected to their karst aquifers. A significant fraction of well-connected karst aquifer storage will be drained by large conduits with short residence times, draining a large portion of the storage every water year. The Blacksmith Fork and American Fork appear to be poorly connected to

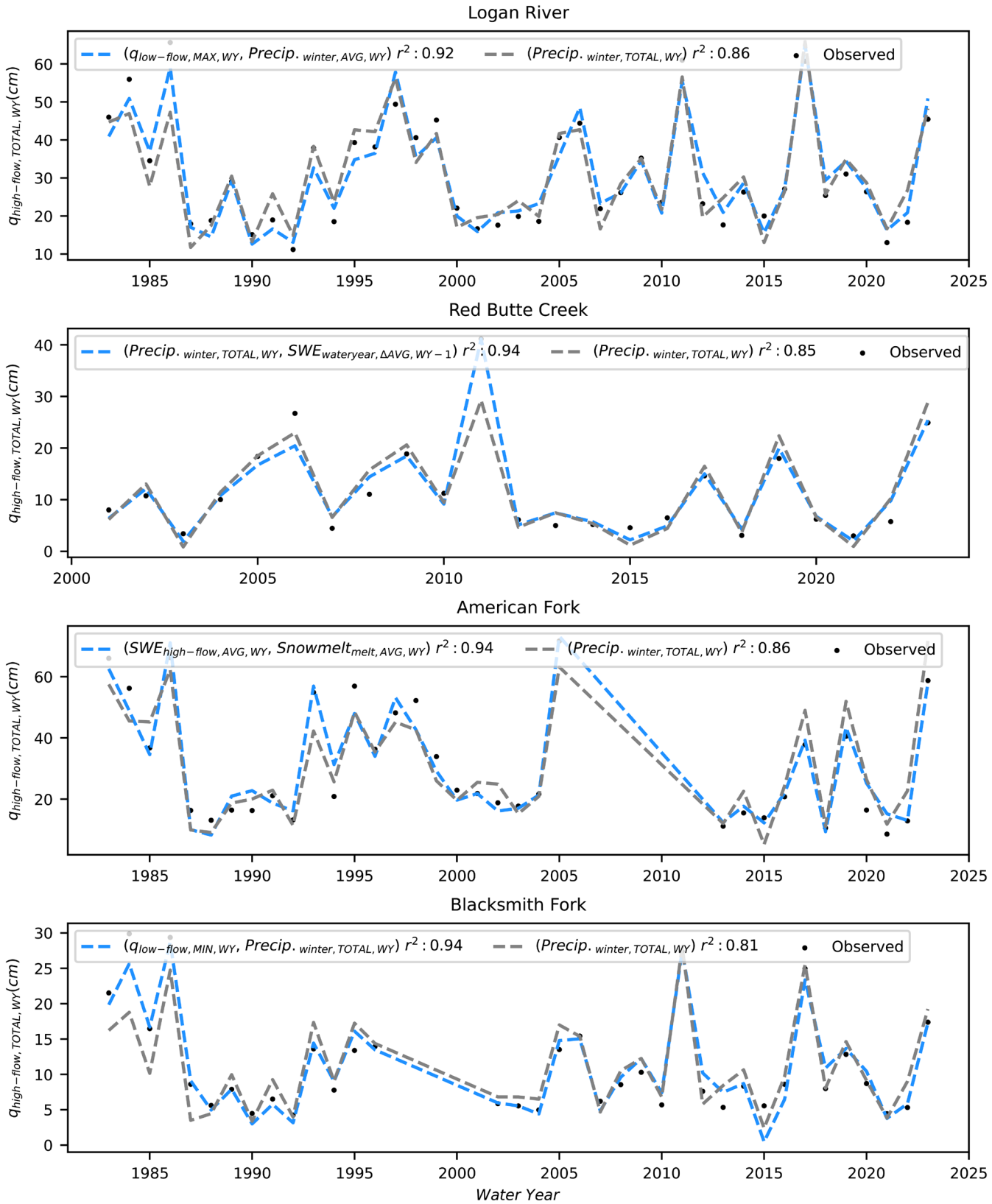

FIGURE 9 | $q_{high\text{-}flow,\ TOTAL,\ WY}$ regression results for the karst watersheds. The blue line shows the prediction results for the variable pair used in the highest rank MLR equation. The grey dotted line shows the regression results for $SWE_{high\text{-}flow,\ AVG,\ WY}$. The observed $q_{high\text{-}flow,\ TOTAL,\ WY}$ values are shown by the black dots.

their karst aquifers. The storage volume connected to the river is reduced, and the karst flow paths are more complex with longer residence times. The predictability of the streamflow regimes in these karst aquifers and clear signals indicating various storage conditions under current climate regimes are of significant benefit to water managers and users.

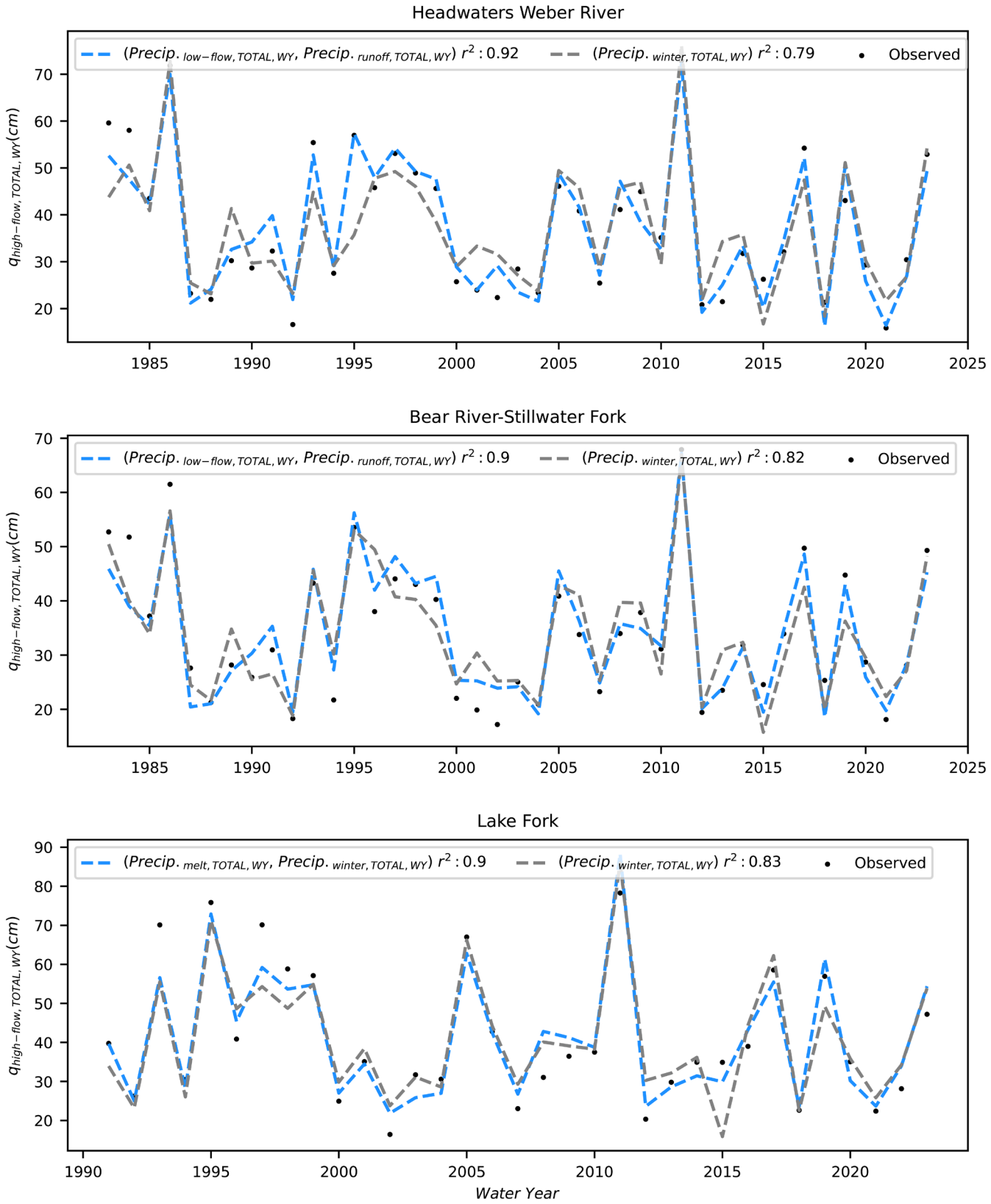

FIGURE 10 | $q_{high\text{-}flow,\ TOTAL,\ WY}$ regression results for the non-karst watersheds. The blue line shows the prediction results for the variable pair used in the highest rank MLR equation. The grey dotted line shows the regression results for $SWE_{high\text{-}flow,\ AVG,\ WY}$. The observed $q_{high\text{-}flow,\ TOTAL,\ WY}$ values are shown by the black dots.

The non-karst watersheds in this study had *high-flow* volumes, $q_{high\text{-}flow,\ TOTAL,\ WY}$, that are also strongly related to and predicted by precipitation metrics (Figures S17–S19, and Table 3 and S7). Again, this is not surprising given the watersheds' high snow fraction (Figure 3). However, in these non-karst watersheds the *low-flow* volumes, $q_{low\text{-}flow,\ TOTAL,\ WY}$, were related to a wide range

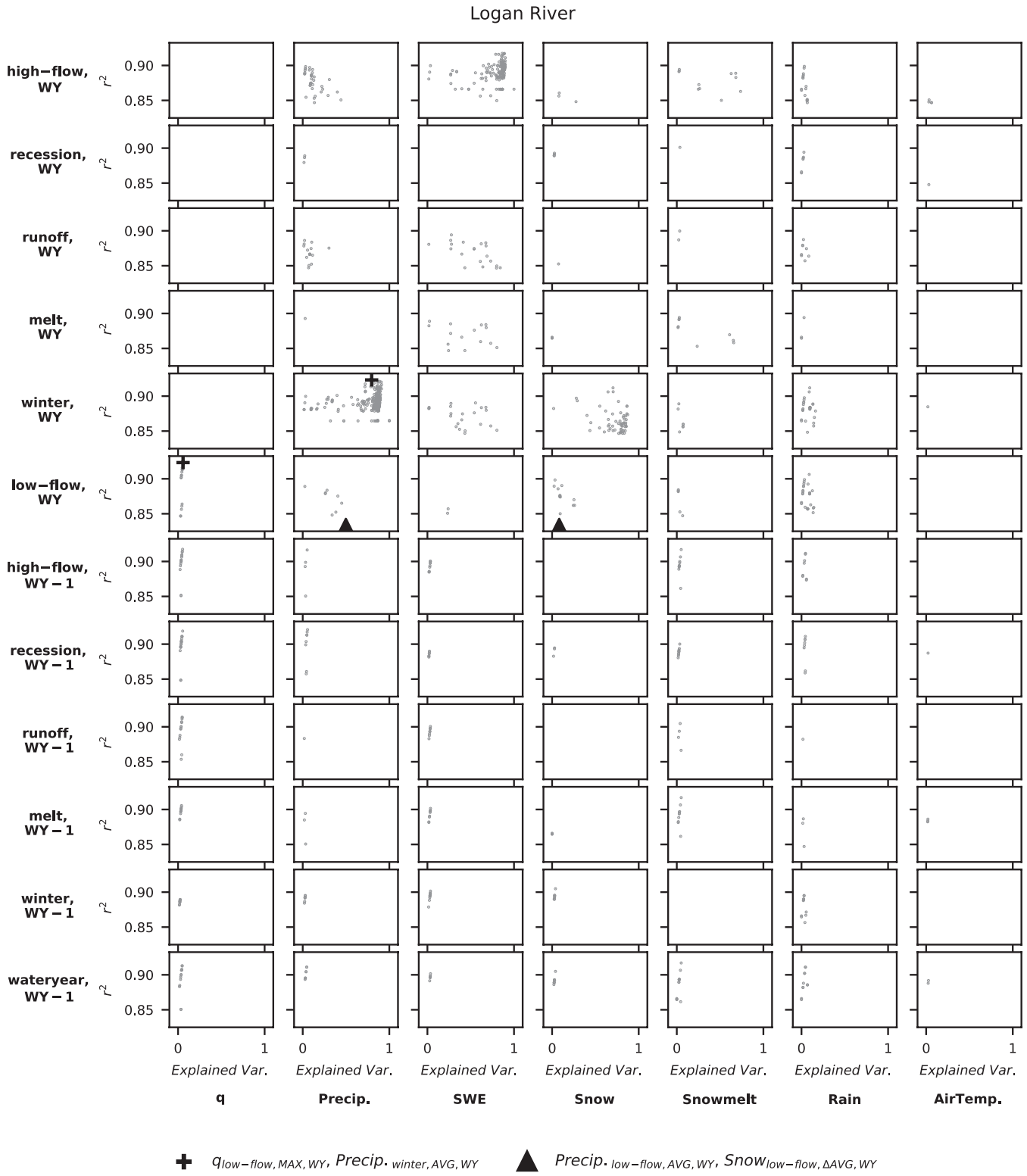

FIGURE 11 | Logan River, MLR equation variables' relationship strength to $q_{high\text{-}flow,\ TOTAL,\ WY}$. Each column of plots represents a different metric, and each row represents a different hydrologic period used in the MLR analysis. Corresponding variables in the top 10% of viable MLR equations are represented in each plot. A plot's y-axis represents the r^2 value of an equation while the x-axis denotes the fraction of explained proportional variance by a given equation variable. The variable pair from the highest ranked equation is represented by "+" s (Figure 9) and variables from the best prediction equation are shown by triangles (Table 3). Variables in all other MLR equations are represented by grey dots.

of metrics, none of which produced good predictive or strong regression equations (Table 2 and S6 and Figures S9–S11). The wide range of weakly related variables indicates complicated hydrologic processes and groundwater storage regimes that could not be represented by the simple and readily available meteorological and hydrologic metrics used in this analysis. Under

TABLE 3 | Best high-flow prediction equations of the form $q_{high\text{-}flow,\ TOTAL,\ WY} = C_1{*}V_1 + C_2{*}V_2 + b$.

Watershed	Coefficient 1 (C_1)	Variable 1 (V_1)	Coefficient 2 (C_2)	Variable 2 (V_2)	Intercept (b)	r^2	RMSE
Logan River (karst)	132.1	$Precip_{low\text{-}flow,\ AVG,\ WY}$	553.0	$Snow_{low\text{-}flow,\ \Delta AVG,\ WY}$	−14.3	0.83	5.79
Red Butte Creek (karst)	105.7	$Precip_{low\text{-}flow,\ AVG,\ WY}$	−7240	$SWE_{water\ year,\ \Delta AVG,\ WY\text{-}1}$	−13.2	0.81	4.01
American Fork (karst)	453.3	$q_{low\text{-}flow,\ AVG,\ WY}$	145.0	$Precip_{low\text{-}flow,\ AVG,\ WY}$	−34.2	0.84	7.56
Blacksmith Fork (karst)	339.3	$q_{low\text{-}flow,\ MIN,\ WY}$	87.8	$Precip_{low\text{-}flow,\ AVG,\ WY}$	−18.3	0.80	3.21
Headwaters Weber River (non-karst)	180.5	$Precip_{low\text{-}flow,\ AVG,\ WY}$	67.3	$Rain_{recession,\ AVG,\ WY\text{-}1}$	−25.3	0.82	6.34
Bear River-Stillwater Fork (non-karst)	2.11	$q_{low\text{-}flow,\ TOTAL,\ WY}$	189.5	$Precip_{low\text{-}flow,\ AVG,\ WY}$	−28.2	0.83	5.19
Lake Fork (non-karst)	220.1	$Precip_{low\text{-}flow,\ AVG,\ WY}$	−4.61	$Snow_{low\text{-}flow,\ MAX,\ WY\text{-}1}$	−0.97	0.77	8.10

current precipitation patterns, the fraction of streamflow volume in the *low-flow* period is a smaller fraction (Figure 3). In contrast, karst aquifers can mimic man-made reservoirs under current precipitation regimes.

Atkinson (1977) showed recharge to karst aquifers was limited during precipitation events by the infiltration rates of the thin soil lenses covering karst flow paths. Infiltration rates in the western karst watersheds will likely be more dynamic under a future rainfall-dominant precipitation regime, as spring runoff currently produces a consistent pattern of saturated soils for an extended period. The streamflow attributable to karst flow paths would likely become more variable across the water year. The karst aquifers would no longer drain in a predictable fashion following spring runoff and the karst contribution to streamflow would become more dependent on soil saturation, evapotranspiration, and amount of rainfall as observed by Iliopoulou et al. (2019). This would produce streamflow regimes in the karst watersheds where the variability would more closely resemble that observed in the *low-flow* periods of the non-karst watersheds and could increase the difficulty of planning and management in karst watersheds.

To facilitate planning under current hydrologic regimes, the predictive equations (Table 3) provide estimates of $q_{high\text{-}flow,\ TOTAL,\ WY}$ for the karst and non-karst watershed studied. These simple equations provide planning insights about potential spring runoff flooding and reservoir filling. In the non-karst watersheds, we are unable to provide reliable predictive equations for $q_{low\text{-}flow,\ TOTAL,\ WY}$. This failure is mitigated by the fact that the rivers studied here flow into large reservoirs immediately downstream and provide a man-made means of moderating low flows. In contrast, the karst watershed *low-flow* periods are being bolstered naturally by the karst aquifer storage. Under current precipitation regimes, $q_{low\text{-}flow,\ TOTAL,\ WY}$ is predictable in the karst watersheds (Table 2). This can assist in anticipating how low flows may get during late summer when demand is high. Under anticipated future climate regimes, streamflow volumes in the karst watersheds will likely become more temporally erratic and require higher temporal resolution precipitation data to be predictable. For watershed managers this would necessitate the development of complex models and/or manageable man-made storage such as reservoirs. Given the extent of karst geology in the western United States and the population's dependence on karst aquifers for water supply, additional efforts should be made to understand the current role karst aquifers are playing in streamflow regimes across the West and how those streamflow regimes might change in response to a changing precipitation regime.

5 | Conclusions

The presence of karst storage in watersheds affects streamflow distribution, resulting in longer recession tails and reduced peak flow compared to non-karst watersheds. Karst watersheds exhibit a "memory effect," where streamflow during dry periods is augmented by water stored in karst aquifers from previous wet periods. This has implications for water management, as it leads to higher flows during droughts and predictable water

availability during critical periods over multiple years. Some sign of a "memory effect" was present in non-karst watersheds, but the predictive power of past flow on *low-flow* volumes was poor and no combination of metrics provided strong predictions, indicating the need for more complicated predictive models.

Future rainfall-dominated precipitation regimes are expected to impact karst aquifers, making streamflow more variable throughout the water year and likely reflecting non-karst watershed streamflow during *low-flow* periods. In both karst and non-karst watersheds, *winter* precipitation is predictive of *high-flow* streamflow volumes. While non-karst watersheds require more complex models to predict *low-flow* volumes, current karst watershed *low-flow* volume is predicted by post peak runoff streamflow. Shifting towards a rainfall-dominated precipitation regime will complicate karst watershed storage and streamflow regimes as aquifer recharge becomes more dependent on the temporal and spatial variability of other hydrologic processes, potentially raising challenges for planning and management in these watersheds.

Acknowledgements

This work was supported with funding from NSF grant #2043363, 2044051, 2043150, and the Utah Water Research Laboratory. All data and code from this study are available on Hydroshare at http://www.hydroshare.org/resource/52aaba03276c4de4943c396fee2363f2.

Data Availability Statement

The data that support the findings of this study are openly available in Hydroshare at https://www.hydroshare.org/resource/52aaba03276c4de4943c396fee2363f2.

References

Addor, N., G. Nearing, C. Prieto, A. J. Newman, N. Le Vine, and M. P. Clark. 2018. "A Ranking of Hydrological Signatures Based on Their Predictability in Space." *Water Resources Research* 54, no. 11: 8792–8812. https://doi.org/10.1029/2018WR022606.

Atkinson, T. C. 1977. "Diffuse Flow and Conduit Flow in Limestone Terrain in the Mendip Hills, Somerset (Great Britain)." *Journal of Hydrology* 35, no. 1: 93–110. https://doi.org/10.1016/0022-1694(77)90079-8.

Bakalowicz, M. 2005. "Karst Groundwater: A Challenge for New Resources." *Hydrogeology Journal* 13, no. 1: 148–160. https://doi.org/10.1007/s10040-004-0402-9.

Bales, R. C., N. P. Molotch, T. H. Painter, M. D. Dettinger, R. Rice, and J. Dozier. 2006. "Mountain Hydrology of the Western United States." *Water Resources Research* 42, no. 8: W08432. https://doi.org/10.1029/2005WR004387.

Barnhart, T. B., N. P. Molotch, B. Livneh, A. A. Harpold, J. F. Knowles, and D. Schneider. 2016. "Snowmelt Rate Dictates Streamflow." *Geophysical Research Letters* 43, no. 15: 8006–8016. https://doi.org/10.1002/2016GL069690.

Barnhart, T. B., C. L. Tague, and N. P. Molotch. 2020. "The Counteracting Effects of Snowmelt Rate and Timing on Runoff." *Water Resources Research* 56, no. 8: e2019WR026634. https://doi.org/10.1029/2019WR026634.

Brooks, P. D., J. Chorover, Y. Fan, et al. 2015. "Hydrological Partitioning in the Critical Zone: Recent Advances and Opportunities for Developing Transferable Understanding of Water Cycle Dynamics." *Water Resources Research* 51, no. 9: 6973–6987. https://doi.org/10.1002/2015WR017039.

Brooks, P. D., A. Gelderloos, M. A. Wolf, et al. 2021. "Groundwater-Mediated Memory of Past Climate Controls Water Yield in Snowmelt-Dominated Catchments." *Water Resources Research* 57, no. 10: e2021WR030605. https://doi.org/10.1029/2021WR030605.

Cochand, M., P. Christe, P. Ornstein, and D. Hunkeler. 2019. "Groundwater Storage in High Alpine Catchments and Its Contribution to Streamflow." *Water Resources Research* 55, no. 4: 2613–2630. https://doi.org/10.1029/2018WR022989.

Dettinger, M., B. Udall, and A. Georgakakos. 2015. "Western Water and Climate Change." *Ecological Applications* 25, no. 8: 2069–2093. https://doi.org/10.1890/15-0938.1.

Dierauer, J. R., P. H. Whitfield, and D. M. Allen. 2018. "Climate Controls on Runoff and Low Flows in Mountain Catchments of Western North America." *Water Resources Research* 54, no. 10: 7495–7510. https://doi.org/10.1029/2018WR023087.

Dieter, C. A., M. A. Maupin, R. R. Caldwell, et al. 2018. "*Estimated Use of Water in the United States in 2015* (Circular No. 1441; Circular)." U.S. Geological Survey.

Doctor, D., J. Jones, N. Wood, J. Falgout, and N. Rapstine. 2020. "Progress Toward a Preliminary Karst Depression Density Map for the Conterminous United States." https://doi.org/10.5038/9781733375313.1003. In *Proceedings of the 16th Multidisciplinary Conference on Sinkholes and the Engineering and Environmental Impacts of Karst*, National Cave and Karst Research Institute Symposium 8, Puerto Rico.

Donovan, K. M., A. E. Springer, B. W. Tobin, and R. A. Parnell. 2022. "Karst Spring Processes and Storage Implications in High Elevation, Semiarid Southwestern United States." In *Threats to Springs in Changing World: Science and Policies for Protection*, American Geophysical Union (AGU). https://doi.org/10.1002/9781119818625.ch4.

Ficklin, D. L., S. M. Robeson, and J. H. Knouft. 2016. "Impacts of Recent Climate Change on Trends in Baseflow and Stormflow in United States Watersheds." *Geophysical Research Letters* 43, no. 10: 5079–5088. https://doi.org/10.1002/2016GL069121.

Fiorillo, F. 2009. "Spring Hydrographs as Indicators of Droughts in a Karst Environment." *Journal of Hydrology* 373, no. 3–4: 290–301. https://doi.org/10.1016/J.JHYDROL.2009.04.034.

Fiorillo, F. 2014. "The Recession of Spring Hydrographs, Focused on Karst Aquifers." *Water Resources Management* 28, no. 7: 1781–1805. https://doi.org/10.1007/S11269-014-0597-Z/FIGURES/9.

Fleming, S. W., and A. G. Goodbody. 2019. "A Machine Learning Metasystem for Robust Probabilistic Nonlinear Regression-Based Forecasting of Seasonal Water Availability in the US West." *IEEE Access* 7: 119943–119964. https://doi.org/10.1109/ACCESS.2019.2936989.

Ford, D., and P. Williams. 2013. *Karst Hydrogeology and Geomorphology*. Chichester, England: John Wiley and Sons Ltd. https://doi.org/10.1002/9781118684986.

Freeze, R. A., and J. A. Cherry. 1979. *Groundwater*. Englewood Cliffs, NJ: Prentice-Hall. http://archive.org/details/groundwater-freeze-and-cherry-1979.

Garen, D. C. 1992. "Improved Techniques in Regression-Based Streamflow Volume Forecasting." *Journal of Water Resources Planning and Management* 118, no. 6: 585–688. https://doi.org/10.1061/(ASCE)0733-9496(1992)118:6(654)?src=getftr.

Gesch, D. B., G. A. Evans, M. J. Oimoen, and S. Arundel. 2018. "The National Elevation Dataset | U.S. Geological Survey." https://www.usgs.gov/publications/national-elevation-dataset.

Godsey, S. E., J. W. Kirchner, and C. L. Tague. 2014. "Effects of Changes in Winter Snowpacks on Summer Low Flows: Case Studies in the Sierra

Nevada, California, USA." *Hydrological Processes* 28, no. 19: 5048–5064. https://doi.org/10.1002/hyp.9943.

Hammond, J. C., A. A. Harpold, S. Weiss, and S. K. Kampf. 2019. "Partitioning Snowmelt and Rainfall in the Critical Zone: Effects of Climate Type and Soil Properties." *Hydrology and Earth System Sciences* 23, no. 9: 3553–3570. https://doi.org/10.5194/HESS-23-3553-2019.

Hammond, J. C., F. A. Saavedra, and S. K. Kampf. 2018. "How Does Snow Persistence Relate to Annual Streamflow in Mountain Watersheds of the Western U.S. With Wet Maritime and Dry Continental Climates?" *Water Resources Research* 54, no. 4: 2605–2623. https://doi.org/10.1002/2017WR021899.

Harpold, A. A., and P. D. Brooks. 2018. "Humidity Determines Snowpack Ablation Under a Warming Climate." *Proceedings of the National Academy of Sciences of the United States of America* 115, no. 6: 1215–1220. https://doi.org/10.1073/pnas.1716789115.

Harrison, H. N., J. C. Hammond, S. Kampf, and L. Kiewiet. 2021. "On the Hydrological Difference Between Catchments Above and Below the Intermittent-Persistent Snow Transition." *Hydrological Processes* 35, no. 11: e14411. https://doi.org/10.1002/HYP.14411.

Hartmann, A., N. Goldscheider, T. Wagener, J. Lange, and M. Weiler. 2014. "Karst Water Resources in a Changing World: Review of Hydrological Modeling Approaches." *Reviews of Geophysics* 52, no. 3: 218–242. https://doi.org/10.1002/2013RG000443.

Hosseini, S. M., B. Ataie-Ashtiani, and C. T. Simmons. 2017. "Spring Hydrograph Simulation of Karstic Aquifers: Impacts of Variable Recharge Area, Intermediate Storage and Memory Effects." *Journal of Hydrology* 552: 225–240. https://doi.org/10.1016/j.jhydrol.2017.06.018.

Iliopoulou, T., C. Aguilar, B. Arheimer, et al. 2019. "A Large Sample Analysis of European Rivers on Seasonal River Flow Correlation and Its Physical Drivers." *Hydrology and Earth System Sciences* 23, no. 1: 73–91. https://doi.org/10.5194/hess-23-73-2019.

Jones, N. A., J. Hansen, A. E. Springer, C. Valle, and B. W. Tobin. 2019. "Modeling Intrinsic Vulnerability of Complex Karst Aquifers: Modifying the COP Method to Account for Sinkhole Density and Fault Location." *Hydrogeology Journal* 27, no. 8: 2857–2868. https://doi.org/10.1007/S10040-019-02056-2/TABLES/4.

Kirchner, J. W. 2016. "Aggregation in Environmental Systems—Part 1: Seasonal Tracer Cycles Quantify Young Water Fractions, But Not Mean Transit Times, in Spatially Heterogeneous Catchments." *Hydrology and Earth System Sciences* 20, no. 1: 279–297. https://doi.org/10.5194/hess-20-279-2016.

Knowles, N., M. D. Dettinger, and D. R. Cayan. 2006. "Trends in Snowfall Versus Rainfall in the Western United States." *Journal of Climate* 19, no. 18: 4545–4559. https://doi.org/10.1175/JCLI3850.1.

Kresic, N. 2012. *Water in Karst: Management, Vulnerability, and Restoration*. Boca Raton, FL: McGraw-Hill Professional. https://doi.org/10.1036/9780071753340.

Labat, D., A. Mangin, and R. Ababou. 2002. "Rainfall–Runoff Relations for Karstic Springs: Multifractal Analyses." *Journal of Hydrology* 256, no. 3–4: 176–195. https://doi.org/10.1016/S0022-1694(01)00535-2.

Land, L., and S. Timmons. 2016. "Evaluation of Groundwater Residence Time in a High Mountain Aquifer System (Sacramento Mountains, USA): Insights Gained From Use of Multiple Environmental Tracers." *Hydrogeology Journal* 24, no. 4: 787–804. https://doi.org/10.1007/s10040-016-1400-4.

Liu, F., R. C. Bales, M. H. Conklin, and M. E. Conrad. 2008. "Streamflow Generation From Snowmelt in Semi-Arid, Seasonally Snow-Covered, Forested Catchments, Valles Caldera, New Mexico." *Water Resources Research* 44, no. 12: W12443. https://doi.org/10.1029/2007WR006728.

Liu, F., M. W. Williams, and N. Caine. 2004. "Source Waters and Flow Paths in an Alpine Catchment, Colorado Front Range, United States." *Water Resources Research* 40, no. 9: W09401. https://doi.org/10.1029/2004WR003076.

Liu, Y., T. Wagener, and A. Hartmann. 2021. "Assessing Streamflow Sensitivity to Precipitation Variability in Karst-Influenced Catchments With Unclosed Water Balances." *Water Resources Research* 57, no. 1: e2020WR028598. https://doi.org/10.1029/2020WR028598.

Mangin, A. 1984. "Pour une meilleure connaissance des systèmes hydrologiques à partir des analyses corrélatoire et spectrale." *Journal of Hydrology* 67, no. 1: 25–43. https://doi.org/10.1016/0022-1694(84)90230-0.

Marshall, A. M., T. E. Link, A. P. Robinson, and J. T. Abatzoglou. 2020. "Higher Snowfall Intensity Is Associated With Reduced Impacts of Warming Upon Winter Snow Ablation." *Geophysical Research Letters* 47, no. 4: e2019GL086409. https://doi.org/10.1029/2019GL086409.

McMillan, H. K. 2021. "A Review of Hydrologic Signatures and Their Applications." *WIREs Water* 8, no. 1: e1499. https://doi.org/10.1002/wat2.1499.

McNamara, J. P., D. Tetzlaff, K. Bishop, et al. 2011. "Storage as a Metric of Catchment Comparison." *Hydrological Processes* 25, no. 21: 3364–3371. https://doi.org/10.1002/hyp.8113.

Meeks, J., and D. Hunkeler. 2015. "Snowmelt Infiltration and Storage Within a Karstic Environment, Vers Chez le Brandt, Switzerland." *Journal of Hydrology* 529: 11–21. https://doi.org/10.1016/j.jhydrol.2015.06.040.

Miller, M. P., D. D. Susong, C. L. Shope, V. M. Heilweil, and B. J. Stolp. 2014. "Continuous Estimation of Baseflow in Snowmelt-Dominated Streams and Rivers in the Upper Colorado River Basin: A Chemical Hydrograph Separation Approach." *Water Resources Research* 50, no. 8: 6986–6999. https://doi.org/10.1002/2013WR014939.

Neilson, B. T., H. Tennant, T. L. Stout, et al. 2018. "Stream Centric Methods for Determining Groundwater Contributions in Karst Mountain Watersheds." *Water Resources Research* 54, no. 9: 6708–6724. https://doi.org/10.1029/2018WR022664.

Nippgen, F., B. L. McGlynn, R. E. Emanuel, and J. M. Vose. 2016. "Watershed Memory at the Coweeta Hydrologic Laboratory: The Effect of Past Precipitation and Storage on Hydrologic Response." *Water Resources Research* 52, no. 3: 1673–1695. https://doi.org/10.1002/2015WR018196.

Pulido-Bosch, A. 2021. *Principles of Karst Hydrogeology*. 1st ed. Cham, Switzerland: Springer International Publishing. https://doi.org/10.1007/978-3-030-55370-8.

Rimmer, A., and Y. Salingar. 2006. "Modelling Precipitation-Streamflow Processes in Karst Basin: The Case of the Jordan River Sources, Israel." *Journal of Hydrology* 331, no. 3: 524–542. https://doi.org/10.1016/j.jhydrol.2006.06.003.

Rumsey, C. A., M. P. Miller, and G. A. Sexstone. 2020. "Relating Hydroclimatic Change to Streamflow, Baseflow, and Hydrologic Partitioning in the Upper Rio Grande Basin, 1980 to 2015." *Journal of Hydrology* 584: 124715. https://doi.org/10.1016/j.jhydrol.2020.124715.

Segura, C., D. Noone, D. Warren, J. A. Jones, J. Tenny, and L. M. Ganio. 2019. "Climate, Landforms, and Geology Affect Baseflow Sources in a Mountain Catchment." *Water Resources Research* 55, no. 7: 5238–5254. https://doi.org/10.1029/2018WR023551.

Sexstone, G. A., D. W. Clow, S. R. Fassnacht, et al. 2018. "Snow Sublimation in Mountain Environments and Its Sensitivity to Forest Disturbance and Climate Warming." *Water Resources Research* 54, no. 2: 1191–1211. https://doi.org/10.1002/2017WR021172.

Sloto, R. A., L. D. Cecil, and L. A. Senior. 1991. "*Hydrogeology and Ground-Water Flow in the Carbonate Rocks of the Little Lehigh Creek Basin, Lehigh County, Pennsylvania* (Water-Resources Investigations Report Nos. 90–4076)." https://doi.org/10.3133/wri904076.U.S. Geological Survey.

Somers, L. D., and J. M. McKenzie. 2020. "A Review of Groundwater in High Mountain Environments." *Wiley Interdisciplinary Reviews: Water* 7, no. 6: e1475. https://doi.org/10.1002/WAT2.1475.

Spangler, L. E. 2001. Delineation of Recharge Areas for Karst Springs in Logan Canyon, Bear River Range, Northern Utah. U.S. Geological Survey, Water-Resources Investigation Report, 01–4011.

Spellman, P., C. Breithaupt, P. Bremner, J. Gulley, J. Jenson, and M. Lander. 2022. "Analyzing Recharge Dynamics and Storage in a Thick, Karstic Vadose Zone." *Water Resources Research* 58, no. 7: e2021WR031704. https://doi.org/10.1029/2021WR031704.

Stewart, I. T., D. R. Cayan, and M. D. Dettinger. 2004. "Changes in Snowmelt Runoff Timing in Western North America Under a 'Business as Usual' Climate Change Scenario." *Climatic Change* 62, no. 1: 217–232. https://doi.org/10.1023/B:CLIM.0000013702.22656.E8.

Tennant, C. J., B. T. Crosby, and S. E. Godsey. 2015. "Elevation-Dependent Responses of Streamflow to Climate Warming." *Hydrological Processes* 29, no. 6: 991–1001. https://doi.org/10.1002/hyp.10203.

The PRISM Climate Group. 2024. *PRISM Gridded Climate Data*. Corvallis, OR: Oregon State University. https://prism.oregonstate.edu/.

Thurber, D., B. Lane, T. Xu, and B. T. Neilson. 2024. "Dissolving the Mystery of Subsurface Controls on Snowmelt–Discharge Dynamics in Karst Mountain Watersheds Using Hydrologic Timeseries." *Hydrological Processes* 38, no. 5: e15170. https://doi.org/10.1002/hyp.15170.

Tobin, B. W., A. E. Springer, D. K. Kreamer, and E. Schenk. 2018. "Review: The Distribution, Flow, and Quality of Grand Canyon Springs, Arizona (USA)." *Hydrogeology Journal* 26, no. 3: 721–732. https://doi.org/10.1007/S10040-017-1688-8/FIGURES/8.

U.S. Army Corps of Engineers. 2024. "National Inventory of Dams." https://nid.sec.usace.army.mil/#/.

U.S. Geological Survey. 2016. *National Water Information System Data Available on the World Wide Web (USGS Water Data for the Nation)*. Reston, VA: U.S. Geological Survey. https://doi.org/10.5066/F7P55KJN.

U.S. Geological Survey. 2024. "Cache Highline Canal Near Logan, Utah—10108400. USGS Water Data for the Nation: U.S. Geological Survey National Water Information System Database." https://waterdata.usgs.gov/monitoring-location/10108400/.

Utah Division of Water Rights. 2024. "Logan City, Dewiit Springs. DVRTVIEW River Commissioner Records Viewer." https://www.waterrights.utah.gov/cgi-bin/dvrtview.exe?Modinfo=StationView&STATION_ID=15.

Vogel, R. M., I. Wilson, and C. Daly. 1999. "Regional Regression Models of Annual Streamflow for the United States." *Journal of Irrigation and Drainage Engineering* 125, no. 3: 148–157. https://doi.org/10.1061/(ASCE)0733-9437(1999)125:3(148).

Winter, T. C. 1995. "Recent Advances in Understanding the Interaction of Groundwater and Surface Water." *Reviews of Geophysics* 33, no. S2: 985–994. https://doi.org/10.1029/95RG00115.

Wolf, M. A., L. R. Jamison, D. K. Solomon, C. Strong, and P. D. Brooks. 2023. "Multi-Year Controls on Groundwater Storage in Seasonally Snow-Covered Headwater Catchments." *Water Resources Research* 59, no. 6: e2022WR033394. https://doi.org/10.1029/2022WR033394.

Worthington, S., G. Schindel, and E. Alexander Jr. 2002. "Techniques for Investigating the Extent of Karstification in the Edwards Aquifer, Texas." *Karst Waters Institue Special Publication* 7: 173–175.

Supporting Information

Additional supporting information can be found online in the Supporting Information section.